



## A long-term numerical solution for the insolation quantities of the Earth

Jacques Laskar, Philippe Robutel, F. Joutel, Mickaël Gastineau, Alexandre C. M. Correia, Benjamin Levrard

### ► To cite this version:

Jacques Laskar, Philippe Robutel, F. Joutel, Mickaël Gastineau, Alexandre C. M. Correia, et al.. A long-term numerical solution for the insolation quantities of the Earth. *Astronomy and Astrophysics* - A&A, 2004, 428, pp.261-285. 10.1051/0004-6361:20041335 . hal-03729629

**HAL Id: hal-03729629**

**<https://hal.science/hal-03729629>**

Submitted on 6 Oct 2022

**HAL** is a multi-disciplinary open access archive for the deposit and dissemination of scientific research documents, whether they are published or not. The documents may come from teaching and research institutions in France or abroad, or from public or private research centers.

L'archive ouverte pluridisciplinaire **HAL**, est destinée au dépôt et à la diffusion de documents scientifiques de niveau recherche, publiés ou non, émanant des établissements d'enseignement et de recherche français ou étrangers, des laboratoires publics ou privés.

# A long-term numerical solution for the insolation quantities of the Earth

J. Laskar<sup>1</sup>, P. Robutel<sup>1</sup>, F. Joutel<sup>1</sup>, M. Gastineau<sup>1</sup>, A. C. M. Correia<sup>1,2</sup>, and B. Levrard<sup>1</sup>

<sup>1</sup> Astronomie et Systèmes Dynamiques, IMCCE – CNRS UMR8028, 77 Av. Denfert-Rochereau, 75014 Paris, France  
e-mail: laskar@imcce.fr

<sup>2</sup> Departamento de Física da Universidade de Aveiro, Campus Universitário de Santiago, 3810-193 Aveiro, Portugal

Received 23 May 2004 / Accepted 11 August 2004

**Abstract.** We present here a new solution for the astronomical computation of the insolation quantities on Earth spanning from –250 Myr to 250 Myr. This solution has been improved with respect to La93 (Laskar et al. 1993) by using a direct integration of the gravitational equations for the orbital motion, and by improving the dissipative contributions, in particular in the evolution of the Earth–Moon System. The orbital solution has been used for the calibration of the Neogene period (Lourens et al. 2004), and is expected to be used for age calibrations of paleoclimatic data over 40 to 50 Myr, eventually over the full Palaeogene period (65 Myr) with caution. Beyond this time span, the chaotic evolution of the orbits prevents a precise determination of the Earth’s motion. However, the most regular components of the orbital solution could still be used over a much longer time span, which is why we provide here the solution over 250 Myr. Over this time interval, the most striking feature of the obliquity solution, apart from a secular global increase due to tidal dissipation, is a strong decrease of about 0.38 degree in the next few millions of years, due to the crossing of the  $s_6 + g_5 - g_6$  resonance (Laskar et al. 1993). For the calibration of the Mesozoic time scale (about 65 to 250 Myr), we propose to use the term of largest amplitude in the eccentricity, related to  $g_2 - g_5$ , with a fixed frequency of  $3.200''/\text{yr}$ , corresponding to a period of 405 000 yr. The uncertainty of this time scale over 100 Myr should be about 0.1%, and 0.2% over the full Mesozoic era.

**Key words.** chaos – celestial mechanics – ephemerides – Earth

## 1. Introduction

Due to gravitational planetary perturbations, the elliptical elements of the orbit of the Earth are slowly changing in time, as is the orientation of the planet’s spin axis. These changes induce variations of the insolation received on the Earth’s surface. The first computation of the secular variations of the Earth’s orbital elements were made by Lagrange (1781, 1782), and then Pontécoulant (1834), but it was the work of Agassiz (1840), showing geological evidence of past ice ages, that triggered the search for a correlation between the geological evidence of large climatic changes, and the variations of the Earth’s astronomical parameters. Shortly after, Adhémar (1842) proposed that these climatic variations originated from the precession of the Earth’s rotation axis.

After the publication of a more precise solution of the Earth by Le Verrier (1856), that took into account the secular perturbations of all main planets except for Neptune, Croll (1890) proposed that the variation of the Earth’s eccentricity was also an important parameter for the understanding of the past climates of the Earth.

The first computations of the variations of the obliquity (angle between the equator and orbital plane) due to the secular variations of the orbital plane of the Earth are due to

Pilgrim (1904), and were later used by Milankovitch (1941) to establish his theory of the Earth’s insolation parameters. Since then, the understanding of the climate response to the orbital forcing has evolved, but all the necessary ingredients for the insolation computations were present in Milankovitch’s work.

The revival of the Milankovitch theory of paleoclimate can be related to the landmark work of Hays et al. (1976), that established a correlation between astronomical forcing and the  $\delta^{18}\text{O}$  records over the past 500 kyr. The Milankovitch theory has since been confirmed overall with variations in the climate response to the insolation forcing (see Imbrie & Imbrie 1979; Imbrie 1982, for more historical details; and Zachos et al. 2001; Grastein et al. 2004, for a recent review on the astronomical calibration of geological data).

Since the work of Pilgrim (1904) and Milankovitch (1941), the orbital and precession quantities of the Earth have undergone several improvements. Le Verrier’s solution (1856) consisted in the linearized equations for the secular evolution of the planetary orbits. Stockwell (1873), and Harzer (1895) added the planet Neptune to Le Verrier’s computations. A significant improvement is due to Hill (1897) who discovered that the proximity of a resonance in Jupiter and Saturn’s motion induces some important complements at the second order with respect to the masses. The solution of

Brouwer & Van Woerkom (1950) is essentially the solution of Le Verrier and Stockwell, complemented by the higher order contributions computed by Hill. This solution was used for insolation computations by Sharav & Boudnikova (1967a,b) with updated values of the parameters, and later on by Vernekar (1972). The computations of Vernekar were actually used by Hays et al. (1976).

The next improvement in the computation of the orbital data is by Bretagnon (1974), who computed the terms of second order and degree 3 in eccentricity and inclination in the secular equations, but omitted the terms of degree 5 in the Jupiter-Saturn system from Hill (1897). This solution was then used by Berger (1978) for the computation of the precession and insolation quantities of the Earth, following Sharav & Boudnikova (1967a,b). All these works assumed implicitly that the motion of the Solar system was regular and that the solutions could be obtained as quasiperiodic series, using perturbation theory.

When Laskar (1984, 1985, 1986) computed in an extensive way the secular equations for the Solar system, including all terms up to order 2 in the masses and 5 in eccentricity and inclination, he realized that the traditional perturbative methods could not be used for the integration of the secular equations, due to strong divergences that became apparent in the system of the inner planets (Laskar 1984). This difficulty was overcome by switching to a numerical integration of the secular equations, which could be done in a very effective way, with a very large stepsize of 500 years. These computations provided a much more accurate solution for the orbital motion of the Solar system (Laskar 1986, 1988), which also included a full solution for the precession and obliquity of the Earth for insolation computations over 10 Myr (million of years). Extending his integration to 200 Myr, Laskar (1989, 1990) demonstrated that the orbital motion of the planets, and especially of the terrestrial planets, is chaotic, with an exponential divergence corresponding to an increase of the error by a factor of 10 every 10 Myr, thus destroying the hope to obtain a precise astronomical solution for paleoclimate studies over more than a few tens of million of years (Laskar 1999).

The first long term direct numerical integration (without averaging) of a realistic model of the Solar system, together with the precession and obliquity equations, was made by Quinn et al. (1991) over 3 Myr. Over its range, this solution presented very small differences with the updated secular solution of Laskar et al. (1993) that was computed over 20 Myr, and has since been extensively used for paleoclimate computations under the acronym La93. The orbital motion of the full Solar system has also been computed over 100 Myr by Sussman & Wisdom (1992), using a symplectic integrator with mixed variables (Wisdom & Holman 1991), confirming the chaotic behaviour found by Laskar (1989, 1990). Following the improvement of computer technology, long term integrations of realistic models of the Solar system become more easy to perform, but are still challenging when the time interval is the age of the Solar system or if the accuracy of the model is comparable to the precision of short term planetary ephemeris. The longest integration was made over several billions of years by Ito & Tanikawa (2002) with a Newtonian model that did not contain general relativity or lunar contributions, while a recent

long term integration of the orbital motion of the Solar system including general relativity, and where the Moon is resolved was made by Varadi et al. (2003) over about 50 Myr.

Here we present the result of the efforts that we have conducted in the past years in our group in order to obtain a new solution for Earth paleoclimate studies over the Neogene period ( $\approx 23$  Myr) and beyond. After a detailed analysis of the main limiting factors for long term integrations (Laskar 1999), and the design of new symplectic integrators (Laskar & Robutel 2001), we have obtained a new numerical solution for both orbital and rotational motion of the Earth that can be used over about 50 Myr for paleoclimate studies, and even over longer periods of time if only the most stable features of the solution are used. Apart from the use of a very complete dynamical model for the orbital motion of the planets, and of the new symplectic integrator of Laskar & Robutel (2001) (see next section), a major change with respect to La93 (Laskar et al. 1993) is the consideration, in the precession solution, of a more complete model for the Earth-Moon tidal interactions (Sect. 4.1).

The present solution (La2004) or some of its previous variants have already been distributed (Laskar 2001) and used for calibration of sedimentary records over extended time interval (Pälike 2002), and in particular for the construction of a new astronomically calibrated geological time scale for the Neogene period (Lourens et al. 2004). The full solution is available on the Web site [www.imcce.fr/Equipes/ASD/insola/earth/earth.html](http://www.imcce.fr/Equipes/ASD/insola/earth/earth.html), together with a set of routines for the computation of the insolation quantities following (Laskar et al. 1993).

In addition to the numerical output of the orbital and rotational parameter of the Earth that is available on the Web site, we have made a special effort to provide in Sect. 8 very compact analytical approximations for the orbital and rotational quantities of the Earth, that can be used in many cases for a better analytical understanding of the insolation variations. Finally, in the last sections, the stability of the solution La2004 is discussed, as well as the possible chaotic transitions of the arguments present in the main secular resonances.

## 2. Numerical model

The orbital solutions La90–93 (Laskar 1990; Laskar et al. 1993) were obtained by a numerical integration of the averaged equations of the Solar system, including the main general relativity and Lunar perturbations. The averaging process was performed using dedicated computer algebra routines. The resulting equations were huge, with about 150 000 polynomial terms, but as the short period terms were no longer present, these equations could be integrated with a step size of 200 to 500 years, allowing very extensive long term orbital computations for the Solar system.

Although these averaged equations solutions could be improved by some new adjustment of the initial conditions and parameters (Laskar et al. 2004), it appears that because of the improvements of computer technology, it becomes now possible to obtain more precise results over a few tens of million of years using a more direct numerical integration of the gravitational equations, and this is how the present new

**Table 1.** Main constants used in La2004. IAU76 refers to the resolutions of the International Astronomical Union of 1976, IERS1992, and IERS2000, refers to the IERS conventions (McCarthy 1992; McCarthy & Petit 2004).

Symbol	Value	Name	Ref.
$\epsilon_0$	84 381.448	Obliquity of the ecliptic at J2000.0	IAU76
$\omega_0$	$7.292115 \times 10^{-5} \text{ rad s}^{-1}$	Mean angular velocity of the Earth at J2000.0	IERS2000
$\psi_0$	5029.0966 ''/cy	Precession constant	IERS2000
$\delta\psi_0$	-0.29965 ''/cy	Correction to the precession	IERS2000
$k_2$	0.305	$k_2$ of the Earth	(Lambeck 1988)
$k_{2M}$	0.0302	$k_2$ of the Moon	(Yoder 1995)
$\Delta t$	639 s	Time lag of the Earth	
$\Delta t_M$	7055 s	Time lag of the Moon	
$J_{2E}$	0.0010826362	Dynamical form-factor for the Earth	IERS1992
$J_{2M}$	0.000202151	Dynamical form-factor for the Moon	IERS1992
$J_{2S}$	$2. \times 10^{-7}$	Dynamical form-factor for the Sun	IERS2000
$R_E$	6378.1366 km	Equatorial radius of the Earth	IERS2000
$R_M$	1738 km	Equatorial radius of the Moon	IAU76
$R_{\text{sun}}$	696 000 000 m	Equatorial radius of the Sun	IAU76
$GS$	$1.32712442076 \times 10^{20} \text{ m}^3 \text{ s}^{-2}$	Heliocentric gravitational constant	IERS2000
$M_{\text{mer}}$	6 023 600	Sun – Mercury mass ratio	IERS1992
$M_{\text{ven}}$	408 523.71	Sun – Venus mass ratio	IERS1992
$M_{\text{ear}}$	328 900.56	Sun – Earth and Moon mass ratio	IERS1992
$M_{\text{mar}}$	3 098 708	Sun – Mars mass ratio	IERS1992
$M_{\text{jup}}$	1047.3486	Sun – Jupiter and satellites mass ratio	IERS1992
$M_{\text{sat}}$	3497.9	Sun – Saturn and satellites mass ratio	IERS1992
$M_{\text{ura}}$	22 902.94	Sun – Uranus and satellites mass ratio	IERS1992
$M_{\text{nep}}$	19 412.24	Sun – Neptune and satellites mass ratio	IERS1992
$M_{\text{plu}}$	135 000 000	Sun – Pluto and Charon mass ratio	IERS1992
$\mu$	0.0123000383	Moon-Earth mass ratio	IERS2000

solution La2004 is obtained. A detailed account of the dynamical equations and numerical integrator is not in the scope of the present paper, but will be made in a forthcoming publication. Nevertheless, we will report here on the main issues concerning the numerical integrator, and will more extensively discuss on the dissipative terms in the integration (see Sect. 4.1).

### 2.1. Dynamical model

The orbital model differs from La93, as it comprises now all 9 planets of the Solar System, including Pluto. The post-Newtonian general relativity corrections of order  $1/c^2$  due to the Sun are included following Saha & Tremaine (1994).

The Moon is treated as a separate object. In order to obtain a realistic evolution of the Earth–Moon system, we also take into account the most important coefficient ( $J_2^S$ ) in the gravitational potential of the Earth and of the Moon (Table 1), and the tidal dissipation in the Earth–Moon System (see Sect. 4.1). We also integrate at the same time the precession and obliquity equations for the Earth and the evolution of its rotation

period in a comprehensive and coherent way, following the lines of Néron de Surgy & Laskar (1997), Correia et al. (2003) (see Sect. 3).

### 2.2. Numerical integrator

In order to minimize the accumulation of roundoff errors, the numerical integration was performed with the new symplectic integrator scheme *SABAC*<sub>4</sub> of (Laskar & Robutel 2001), with a correction step for the integration of the Moon. This integrator is particularly adapted to perturbed systems where the Hamiltonian governing the equations of motion can be written in the form  $H = A + \epsilon B$ , as the sum of an integrable part  $A$  (the Keplerian equations of the planets orbiting the Sun and of the Moon around the Earth), and a small perturbation potential  $\epsilon B$  (here the small parameter  $\epsilon$  is of the order of the planetary masses). Using this integrator with step size  $\tau$  is then equivalent to integrate exactly a close by Hamiltonian  $\tilde{H}$ , where the error of method  $H - \tilde{H}$  is of the order of  $O(\tau^8 \epsilon) + O(\tau^2 \epsilon^2)$ , and even  $O(\tau^8 \epsilon) + O(\tau^4 \epsilon^2)$  when the correction step is added,

while the same quantity is of the order  $O(\tau^2\epsilon)$ , in the widely used symplectic integrator of (Wisdom & Holman 1991). More precisely, the integration step  $S_0(\tau)$  with *SABA*<sub>4</sub> is

$$S_0(\tau) = e^{\tau c_1 L_A} e^{\tau d_1 L_B} e^{\tau c_2 L_A} e^{\tau d_2 L_B} e^{\tau c_3 L_A} \times e^{\tau d_3 L_B} e^{\tau c_4 L_A} e^{\tau d_4 L_B} e^{\tau c_5 L_A} \quad (1)$$

where  $\tau$  is the integration step,  $L_f$  is the differential operator defined by  $L_f g = \{f, g\}$ , where  $\{f, g\}$  is the usual Poisson bracket, and the coefficients  $c_i$  and  $d_i$  are

$$\begin{aligned} c_1 &= 1/2 - \sqrt{525 + 70\sqrt{30}}/70 \\ c_2 &= \left( \sqrt{525 + 70\sqrt{30}} - \sqrt{525 - 70\sqrt{30}} \right) / 70 \\ c_3 &= \left( \sqrt{525 - 70\sqrt{30}} \right) / 35 \end{aligned} \quad (2)$$

$$d_1 = 1/4 - \sqrt{30}/72$$

$$d_2 = 1/4 + \sqrt{30}/72.$$

For the integration of the Earth–Moon system, we have added a correction step (see Laskar & Robutel 2001), and the full integrator steps  $S_1(\tau)$  of *SABAC*<sub>4</sub> then becomes

$$S_1(\tau) = e^{-\tau^3 \epsilon^2 b / 2L_C} S_0(\tau) e^{-\tau^3 \epsilon^2 b / 2L_C} \quad (3)$$

where  $b = 0.00339677504820860133$  and  $C = \{A, B, B\}$ . The step size used in the integration was  $\tau = 5 \times 10^{-3}$  yr = 1.82625 days. The initial conditions of the integration were least square adjusted to the JPL ephemeris DE406, in order to compensate for small differences in the model. In particular, we do not take into account the effect of the minor planets, and the modelization of the body interactions in the Earth–Moon system is more complete in DE406 (see Williams et al. 2001). The integration time for our complete model, with  $\tau = 5 \times 10^{-3}$  yr is about one day per 5 Myr on a Compaq Alpha (ev68, 833 Mhz) workstation.

### 2.3. Numerical roundoff error

In Fig. 1a is plotted the evolution of the total energy of the system from  $-250$  Myr to  $+250$  Myr. The energy presents a secular trend that corresponds to the dissipation in the Earth–Moon system. Indeed, after removing the computed energy change due to the secular evolution of the Earth–Moon semi-major axis, the secular trend in the energy evolution disappears and we are left with a residual that is smaller than  $2.5 \times 10^{-10}$  after 250 Myr, and seems to behave as a random walk (Fig. 1b). The normal component of the angular momentum is conserved over the same time with a relative error of less than  $1.3 \times 10^{-10}$  (Fig. 1c).

In order to test the randomness of the numerical error in the integration, we have plotted the distribution of the difference of total energy from one 1000 year step to the next. After normalization to 1 of the area of the distribution curve (Fig. 2), we obtain a curve that is almost identical to the normalized Gaussian function

$$f(t) = \frac{1}{\sigma \sqrt{2\pi}} \exp\left(-\frac{x^2}{2\sigma^2}\right) \quad (4)$$

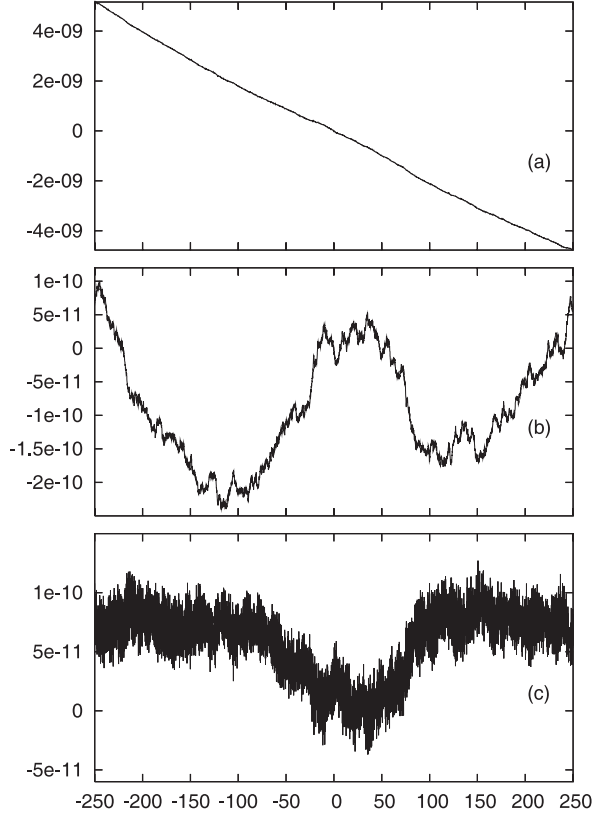


**Fig. 1.** Conservation of integrals. **a)** Relative variation of the total energy of the system versus time (in Myr) from  $-250$  Myr to  $+250$  Myr. **b)** The same after correction of the secular trend due to the tidal dissipation in the Earth–Moon system. **c)** Relative variation of the normal component of the total angular momentum.

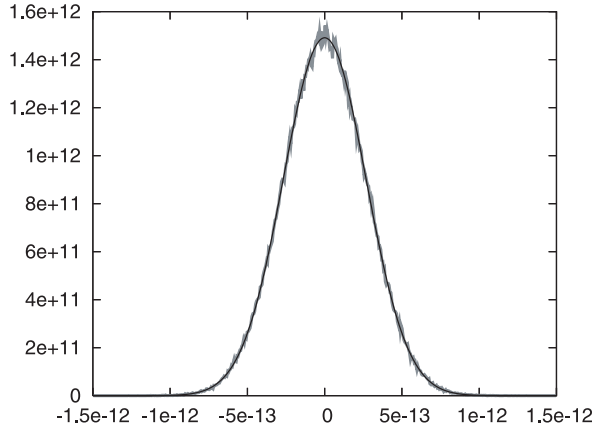


**Fig. 2.** Normalized repartition of the energy numerical error for 1000 yr steps, over the whole integration, from  $-250$  Myr to  $+250$  Myr. Practically superposed to this curve is the computed normal distribution given by Eqs. (4) and (5).

where  $\sigma = 2.6756 \times 10^{-13}$  is the computed standard deviation

$$\sigma = \sqrt{\sum_i (x_i - m)^2 / (N - 1)} \quad (5)$$

while the mean  $m = -2.6413 \times 10^{-18}$  is neglected. The integration stepsize is  $5 \times 10^{-3}$  yr, the standard deviation per step is thus  $\sigma_1 = 5.9828 \times 10^{-16}$ , that is about  $2.7\epsilon_M$ ,

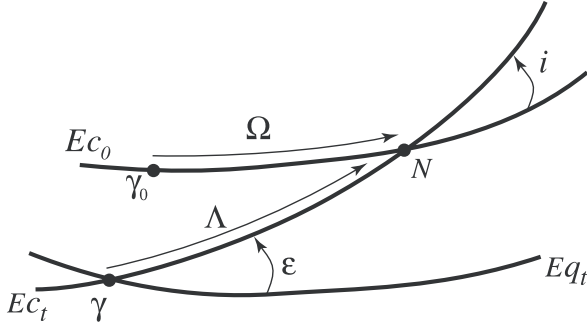


**Fig. 3.** Fundamental planes for the definition of precession and obliquity.  $E_{q_t}$  and  $E_{c_t}$  are the mean equator and ecliptic at date  $t$ .  $E_{c_0}$  is the fixed ecliptic at Julian date J2000, with equinox  $\gamma_0$ . The general precession in longitude  $\psi$  is defined by  $\psi = \Lambda - \Omega$ .  $\omega$  is the longitude of the node, and  $i$  the inclination. The angle  $\varepsilon$  between  $E_{q_t}$  and  $E_{c_t}$  is the obliquity.

where  $\varepsilon_M \approx 2.22 \times 10^{-16}$  is the machine Epsilon in double precision. Assuming that the machine error is uniformly distributed in the interval  $[-\varepsilon_M/2, +\varepsilon_M/2]$ , the standard error of an elementary operation is  $\sigma_0 = \varepsilon_M/\sqrt{12}$ , and the error over one step thus corresponds to  $(\sigma_1/\sigma_0)^2 \approx 87$  elementary operations. This value is thus extremely small, and we believe that we will not be able to improve  $\sigma_1$  unless we decrease  $\sigma_0$  by switching to higher machine precision. For example, in quadruple precision (128 bits for the representation of a real number),  $\varepsilon_M \approx 1.93 \times 10^{-34}$ . Moreover, the Gaussian distribution of the increments of the energy (Fig. 2) ensures that we do not have systematic trends in our computations, and that the numerical errors behave as a random variable with zero mean. The total energy error reflects mostly the behavior of the outer planets, but we can assume that the numerical error will behave in roughly the same for all the planets, although for Mercury, due to its large eccentricity, some slight increase of the error may occur. This should not be the case for the error of method, resulting from the truncation in power of  $\tau$  in the integrator, where the error should decrease as the period of the planet increases.

### 3. Precession equations

We suppose here that the Earth is a homogeneous rigid body with moments of inertia  $A < B < C$  and we assume that its spin axis is also the principal axis of inertia. The precession  $\psi$  and obliquity  $\varepsilon$  (Fig. 3) equations for the rigid Earth in the presence of planetary perturbations are given by Kinoshita (1977), Laskar (1986), Laskar et al. (1993), Néron de Surgy & Laskar (1997).

$$\begin{cases} \frac{dX}{dt} = L \sqrt{1 - \frac{X^2}{L^2}} (\mathcal{B}(t) \sin \psi - \mathcal{A}(t) \cos \psi) \\ \frac{d\psi}{dt} = \frac{\alpha X}{L} - \frac{X}{L \sqrt{1 - \frac{X^2}{L^2}}} (\mathcal{A}(t) \sin \psi + \mathcal{B}(t) \cos \psi) - 2C(t). \end{cases} \quad (6)$$

With  $X = \cos \varepsilon$ ,  $L = C\omega$ , where  $\omega$  is the spin rate of the Earth, and

$$\begin{cases} \mathcal{A}(t) = \frac{2}{\sqrt{1 - p^2 - q^2}} [\dot{q} + p(q\dot{p} - p\dot{q})] \\ \mathcal{B}(t) = \frac{2}{\sqrt{1 - p^2 - q^2}} [\dot{p} - q(q\dot{p} - p\dot{q})] \\ C(t) = q\dot{p} - p\dot{q} \end{cases} \quad (7)$$

where  $q = \sin(i/2) \cos \Omega$  and  $p = \sin(i/2) \sin \Omega$ , and where  $\alpha$  is the “precession constant”:

$$\alpha = \frac{3G}{2\omega} \left[ \frac{m_\odot}{(a_\odot \sqrt{1 - e_\odot^2})^3} + \frac{m_M}{(a_M \sqrt{1 - e_M^2})^3} \left( 1 - \frac{3}{2} \sin^2 i_M \right) \right] E_d. \quad (8)$$

For a fast rotating planet like the Earth, the dynamical ellipticity  $E_d = (2C - A - B)/C$  can be considered as proportional to  $\omega^2$ ; this corresponds to the hydrostatic equilibrium (see for example Lambeck 1980). In this approximation,  $\alpha$  is thus proportional to  $\omega$ . The quantities  $\mathcal{A}$ ,  $\mathcal{B}$  and  $C$  are related to the secular evolution of the orbital plane of the Earth and are given by the integration of the planetary motions.

## 4. Contributions of dissipative effects

### 4.1. The body tides

#### 4.1.1. Rotational evolution

Following (Darwin 1880; Mignard 1979), we assume that the torque resulting from tidal friction is proportional to the time lag  $\Delta t$  needed for the deformation to reach the equilibrium. This time lag is supposed to be constant, and the angle between the direction of the tide-raising body and the direction of the high tide (which is carried out of the former by the rotation of the Earth) is proportional to the speed of rotation. Such a model is called “viscous”, and corresponds to the case for which  $1/Q$  is proportional to the tidal frequency.

After averaging over the mean anomaly of the Moon and Earth (indices  $M$  and  $\oplus$ ), and over the longitude of node and perigee of the Moon, we have at second order in eccentricity for the contributions of the solar tides

$$\begin{cases} \frac{dL}{dt} = -\frac{3Gm_\odot^2 R^5 k_2 \Delta t}{2a_\odot^6} \times \left[ \left( 1 + \frac{15}{2} e_\odot^2 \right) \left( 1 + \frac{X^2}{L^2} \right) \frac{L}{C} - 2 \left( 1 + \frac{27}{2} e_\odot^2 \right) \frac{X}{L} n_\odot \right] \\ \frac{dX}{dt} = -\frac{3Gm_\odot^2 R^5 k_2 \Delta t}{2a_\odot^6} \times \left[ 2 \left( 1 + \frac{15}{2} e_\odot^2 \right) \frac{X}{C} - 2 \left( 1 + \frac{27}{2} e_\odot^2 \right) n_\odot \right] \end{cases} \quad (9)$$

where  $n_\odot$  is the mean motion of the Sun (index  $\odot$ ) around the Earth, while the contribution of the lunar tides is

$$\left\{ \begin{array}{l} \frac{dL}{dt} = -\frac{3Gm_M^2 R^5 k_2 \Delta t}{2a_M^6} \\ \times \left[ \frac{1}{2} \left( 1 + \frac{15}{2} e_M^2 \right) \left[ 3 - \cos^2 i_M + (3 \cos^2 i_M - 1) \frac{X^2}{L^2} \right] \frac{L}{C} \right. \\ \left. - 2 \left( 1 + \frac{27}{2} e_M^2 \right) \frac{X}{L} n_M \cos i_M \right] \\ \frac{dX}{dt} = -\frac{3Gm_M^2 R^5 k_2 \Delta t}{2a_M^6} \\ \times \left[ \left( 1 + \frac{15}{2} e_M^2 \right) (1 + \cos^2 i_M) \frac{X}{C} \right. \\ \left. - 2 \left( 1 + \frac{27}{2} e_M^2 \right) n_M \cos i_M \right]. \end{array} \right. \quad (10)$$

The “cross tides”, are obtained by the perturbation of the tidal bulge raised by the Sun or the Moon on the other body. Their importance was noticed by Touma & Wisdom (1994). These tidal effects tend to drive the equator towards the ecliptic, and have both the same magnitude

$$\left\{ \begin{array}{l} \frac{dL}{dt} = -\frac{3Gm_\odot m_M R^5 k_2 \Delta t}{4a_\odot^3 a_M^3} \\ \times \left( 1 + \frac{3}{2} e_\odot^2 \right) \left( 1 + \frac{3}{2} e_M^2 \right) (3 \cos^2 i_M - 1) \left( 1 - \frac{X^2}{L^2} \right) \frac{L}{C} \\ \frac{dX}{dt} = 0. \end{array} \right. \quad (11)$$

#### 4.1.2. Orbital evolution

At second order in eccentricity, we have for the orbital evolution of the Moon (Mignard 1979, 1980, 1981; Néron de Surgy & Laskar 1997)

$$\left\{ \begin{array}{l} \frac{da_M}{dt} = \frac{6Gm_M^2 R^5 k_2 \Delta t}{\mu a_M^7} \\ \times \left[ \left( 1 + \frac{27}{2} e_M^2 \right) \frac{X}{C n_M} \cos i_M - (1 + 23 e_M^2) \right] \\ \frac{de_M}{dt} = \frac{3Gm_M^2 R^5 k_2 \Delta t e_M}{\mu a_M^8} \left[ \frac{11}{2} \frac{X}{C n_M} \cos i_M - 9 \right] \\ \frac{d \cos i_M}{dt} = \frac{3Gm_M^2 R^5 k_2 \Delta t}{2\mu a_M^8} (1 + 8 e_M^2) \frac{X}{C n_M} \sin^2 i_M \end{array} \right. \quad (12)$$

where  $\mu = m_\oplus m_M / (m_\oplus + m_M)$ , and for the Sun

$$\left\{ \begin{array}{l} \frac{da_\odot}{dt} = \frac{6Gm_\odot^2 R^5 k_2 \Delta t}{\mu' a_\odot^7} \\ \times \left[ \left( 1 + \frac{27}{2} e_\odot^2 \right) \frac{X}{C n_\odot} - (1 + 23 e_\odot^2) \right] \\ \frac{de_\odot}{dt} = \frac{3Gm_\odot^2 R^5 k_2 \Delta t e_\odot}{\mu' a_\odot^8} \left[ \frac{11}{2} \frac{X}{C n_\odot} - 9 \right] \end{array} \right. \quad (13)$$

where  $\mu' = m_\oplus m_\odot / (m_\oplus + m_\odot)$ . However, both last variations are negligible: about 3 meters per Myr for  $da_\odot/dt$  and  $10^{-12}$  per Myr for  $de_\odot/dt$ .

#### 4.1.3. Tides on the Moon

We have also taken into account the tidal effect raised by the Earth on the Moon, following Néron de Surgy & Laskar (1997), with the following simplifying assumptions that the Moon is locked in synchronous spin-orbit resonance with the Earth (i.e.  $\omega_M = n_M$ ), and expanding only at first order in the Moon inclination ( $6.41^\circ$  at  $t = J2000$ ). We thus obtain the additional contributions

$$\left\{ \begin{array}{l} \frac{da_M}{dt} = -\frac{57Gm_\oplus^2 R_M^5 k_{2M} \Delta t e_M^2}{\mu a_M^7} \\ \frac{de_M}{dt} = -\frac{21Gm_\oplus^2 R_M^5 k_{2M} \Delta t e_M}{2\mu a_M^8}. \end{array} \right. \quad (14)$$

With the numerical values from Table 1, these contributions represent 1.2% of the total  $da_M/dt$  and 30% of the total  $de_M/dt$  for present conditions. Finally, the tides raised on the Moon by the Sun can be neglected because the ratio of the magnitudes of solar and terrestrial tides on the Moon is

$$\left( \frac{m_\odot}{m_\oplus} \right)^2 \left( \frac{a_\odot}{a_M} \right)^6 \simeq 3.2 \times 10^{-5}. \quad (15)$$

#### 4.2. Other dissipative effects

##### 4.2.1. Core-mantle friction

The core and the mantle have different dynamical ellipticities, so they tend to have different precession rates. This trend produces a viscous friction at the core-mantle boundary (Poincaré 1910; Rochester 1976; Lumb & Aldridge 1991). We will consider here that an effective viscosity  $\nu$  can account for a weak laminar friction, as well as a strong turbulent one which thickens the boundary layer (e.g. Correia et al. 2003).

The core-mantle friction tends to slow down the rotation and to bring the obliquity down to  $0^\circ$  if  $\varepsilon < 90^\circ$  and up to  $180^\circ$  otherwise, which contrasts with the effect of the tides. Furthermore, one can see that, despite the strong coupling by pressure forces, there can be a substantial contribution to the variation of the spin for high viscosities and moderate speeds of rotation.

##### 4.2.2. Atmospheric tides

The Earth’s atmosphere also undergoes some torques which can be transmitted to the surface by friction: a torque caused by the gravitational tides raised by the Moon and the Sun, a magnetic one generated by interactions between the magnetosphere and the solar wind. Both effects are negligible; see respectively Chapman & Lindzen (1970) and Volland (1978).

Finally, a torque is produced by the daily solar heating which induces a redistribution of the air pressure, mainly driven by a semidiurnal wave, hence the so-called thermal atmospheric tides (Chapman & Lindzen 1970). The axis of symmetry of the resulting bulge of mass is permanently shifted out of the direction of the Sun by the Earth’s rotation. As for the body tides, this loss of symmetry is responsible for the torque which, in the present conditions, tends to accelerate the spin (Correia & Laskar 2003).



Volland (1978) showed that this effect is not negligible, reducing the Earth's despinning by about 7.5%. But, although the estimate of their long term contributions deserves careful attention, we have not taken the atmospheric tides into account in the computations presented in the next sections, assuming that, as the uncertainty on some of the other factors is still large, the global results obtained here will not differ much when taking this additional effect into consideration.

#### 4.2.3. Mantle convection

Several internal geophysical processes are able to affect the moments of inertia of the Earth and thereby its precession constant value. Redistribution of mass within the Earth can occur as a consequence of plate subduction, upwelling plumes, mantle avalanches or density anomalies driven by mantle convection. Typical time-scales of these phenomena range from  $\sim 10$  to 100 Myr. However, their impact is still poorly known. Forte & Mitrovia (1997) computed convection-induced perturbations in the dynamical ellipticity of the Earth over the last 20 Myr, using different sets of 3D seismic heterogeneity models and mantle viscosity profiles. Most of the models indicate that mantle convection led to a mean relative increase of the precession constant close to  $\sim 0.5\%$  since the beginning of the Neogene period ( $\sim 23$  Myr ago). Although this value is similar to our estimate of the tidal dissipation effect (but in the opposite direction, see Sect. 9), we did not take account of its impact in our computations. Because of its still large uncertainty, we feel that it is more appropriate to include its possible contribution as a perturbation of the tidal dissipation parameter.

#### 4.2.4. Climate friction

Climate friction is a positive and dissipative feedback between obliquity variations and climate which may cause a secular drift of the spin axis. In response to quasi-periodic variations in the obliquity, glacial and interglacial conditions drive transport of water into and out of the polar regions, affecting the dynamical ellipticity of the Earth. A significant fraction of the surface loading is compensated by viscous flow within the Earth, but delayed responses in both climatic and viscous relaxation processes may introduce a secular term in the obliquity evolution (Rubincam 1990, 1995). Because both the ice load history and the visco-elastic structure of the Earth are not strongly constrained, it is difficult to produce accurate simulations and predictions of the coupled response of the entire system. Nevertheless, simplifying assumptions have been used to estimate the magnitude and the direction of the secular drift. Several analyses have examined this phenomenon, suggesting that climate friction could have changed the Earth's obliquity by more than  $20^\circ$  over its whole geological history (Bills 1994; Ito et al. 1995; Williams et al. 1998). A more detailed theoretical and numerical treatment of climate friction has been developed by Lévraud & Laskar (2003). Using available constraints on the ice volume response to obliquity forcing based on  $\delta^{18}\text{O}$  oxygen-isotope records, they showed that climate friction impact is likely negligible. Over the last 3 Ma,

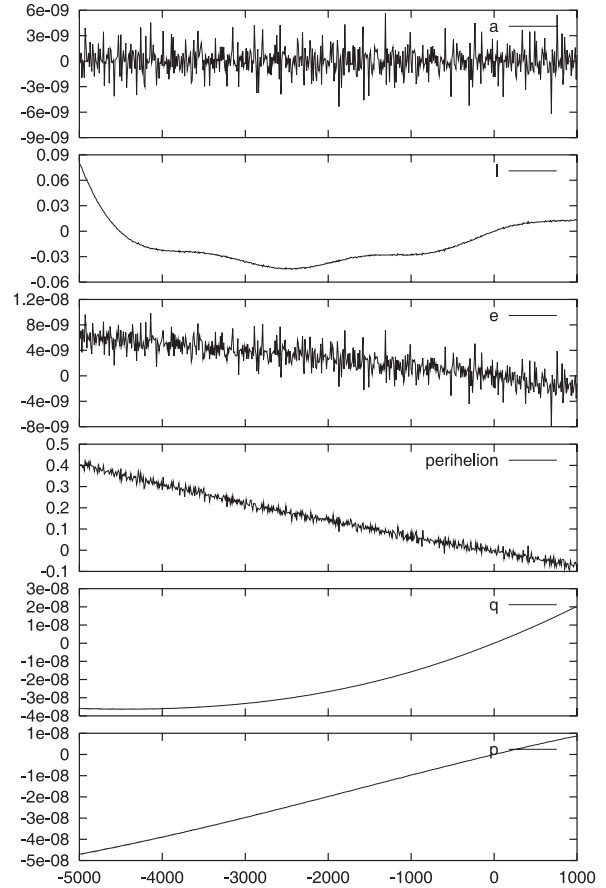


**Fig. 4.** Differences La2003-DE406 over the full range of DE406 ( $-5000$  yr to  $+1000$  from J2000). The units for semi-major axis ( $a$ ) are AU, arcsec for mean longitude ( $l$ ) and longitude of perihelion (perihelion). The eccentricity ( $e$ ) and the inclinations variables ( $q = \sin(i/2) \cos(\Omega)$ ,  $p = \sin(i/2) \sin(\Omega)$ ), where  $i$  and  $\Omega$  are the inclination and node from the ecliptic and equinox J2000.

corresponding to the intensification of the Northern Hemisphere glaciation, a maximal absolute drift of only  $\sim 0.04^\circ/\text{Myr}$  has been estimated for a realistic lower mantle viscosity of  $10^{22}$  Pa. s. Before 3 Ma, climate friction impact is expected to be much more negligible because of the lack of massive ice caps. In this context, this effect was not taken into account in our long-term computations. Indeed, the uncertainty on the tidal dissipation is still important and it is expected that most of the possible effect of climate friction would be absorbed by a small change of the main tidal dissipation parameters.

Nevertheless, glaciation-induced perturbations in the dynamical ellipticity of the Earth change the precession frequency and thereby the obliquity frequencies leading to a temporal shift between a perturbed and a nominal solution (see Sect. 9). Estimates of this offset have been performed by Mitrovia & Forte (1995) and Lévraud & Laskar (2003) for a large set of mantle viscosity profiles. It may reach between  $\sim 0.7$  and 8 kyr after 3 Myr, corresponding respectively to extreme lower mantle viscosities of  $3 \times 10^{21}$  and  $10^{23}$  Pa. s. In the last case, the Earth is nearly rigid on orbital timescales and the corresponding offset can be thus reasonably considered as a maximal value.



## 5. Comparison with DE406

Using a direct numerical integrator, our goal is to provide a long term solution for the orbital and precessional elements of the Earth with a precision that is comparable with the usual accuracy of a short time ephemeris. We have thus compared our solution with the most advanced present numerical integration, DE406, that was itself adjusted to the observations (Standish 1998). Over the full range of DE406, that is from  $-5000$  yr to  $+1000$  yr from the present date, the maximum difference in the position of the Earth–Moon barycenter is less than  $0.09$  arcsec in longitude, and the difference in eccentricity less than  $10^{-8}$ . The difference in the longitude of the Moon are more important, as the dissipative models that are used in the two integrations are slightly different. They amount to  $240$  arcsec after  $5000$  years, and the eccentricity difference is of the order of  $2 \times 10^{-5}$ , but it should be noted that only the averaged motion of the Moon will have some significant influence on the precession and obliquity of the Earth. Table 2 summarizes the maximum differences between La2004 and DE406 for the main orbital elements, over the whole interval of DE406, for different time intervals.

## 6. Comparison with La93

We have compared in Figs. 5 and 6 the eccentricity and inclination of the secular solution La93 and the new present solution La2004. Over  $10$  Myr, the two orbital solutions La93 and La2004 are nearly identical, and do not differ significantly over  $20$  Myr. The differences in eccentricity increase regularly with time, amounting to about  $0.02$  in the eccentricity after  $20$  Myr, about  $1/3$  of the total amplitude  $\approx 0.063$ , while the difference in the orbital inclination reaches  $1$  degree, to compare to a maximum variation of  $4.3$  degrees. These differences result mostly from a small difference in the main secular frequency  $g_6$  from Jupiter and Saturn that is now  $g_6 = 28.2450$  arcsec/year (Table 3) instead of  $28.2207$  arcsec/year in the previous solution. Beyond  $20$  million years, the differences between the two solutions become more noticeable. The solutions in obliquity and climatic precession are plotted in Figs. 7 and 8. The difference in obliquity over  $20$  Myr amounts to about  $2$  degrees, which means that the obliquity cycles of the two solutions become nearly out of phase after this date. The differences La2004–La93 are plotted in (a), while in (b) only the precession model has been changed and in (c) only the orbital model has been changed. Comparing 7b and 7c shows that most of the differences between the La93 and La2004 obliquity solutions result from the change in the dissipative model of the Earth–Moon system, while the only change of the orbital solution would lead to a much smaller change of only  $0.6$  degree in obliquity after  $20$  Myr. Similar conclusions can be made for the climatic precession (Figs. 8a–c).

## 7. Secular frequencies

Over long time scales, the determination of longitude of the planet on its orbit is not very important, and we are more concerned by the slow evolution of the Earth orbit under secular planetary perturbations. The semi-major axis of the Earth

**Table 2.** Maximum difference between La2004 and DE406 over the whole time interval of DE406 ( $-5000$  yr to  $+1000$  yr with origin at J2000); Col. 1:  $-100$  to  $+100$  yr; Col. 2:  $-1000$  to  $+1000$  yr; Col. 3:  $-5000$  to  $+1000$  yr. EMB is the Earth–Moon barycenter.

$\lambda ('' \times 1000)$			
Mercury	8	60	90
Venus	12	107	143
EMB	3	28	79
Mars	19	171	277
Jupiter	5	69	69
Saturn	1	4	7
Uranus	1	3	4
Neptune	2	7	16
Pluto	3	9	17
Moon	13 470	85 873	221 724
Earth	10	88	238
$a (\text{UA} \times 10^{10})$			
Mercury	4	43	58
Venus	13	23	27
EMB	29	62	62
Mars	27	76	76
Jupiter	268	470	565
Saturn	743	1073	1168
Uranus	1608	3379	3552
Neptune	3315	5786	6458
Pluto	4251	10 603	10 603
Moon	23	204	520
Earth	487	3918	10 238
$e (\times 10^{10})$			
Mercury	33	52	144
Venus	12	33	103
EMB	30	80	98
Mars	62	130	468
Jupiter	30	95	158
Saturn	69	107	138
Uranus	99	135	144
Neptune	65	177	201
Pluto	92	215	215
Moon	11 152	252 832	252 832
Earth	460	3669	8694
$\sin(i/2) (\times 10^{10})$			
Mercury	2	18	88
Venus	5	55	144
EMB	17	190	414
Mars	48	492	2053
Jupiter	1	11	122
Saturn	1	6	100
Uranus	2	5	5
Neptune	2	6	6
Pluto	5	13	17
Moon	5765	97 275	600 789
Earth	19	202	841

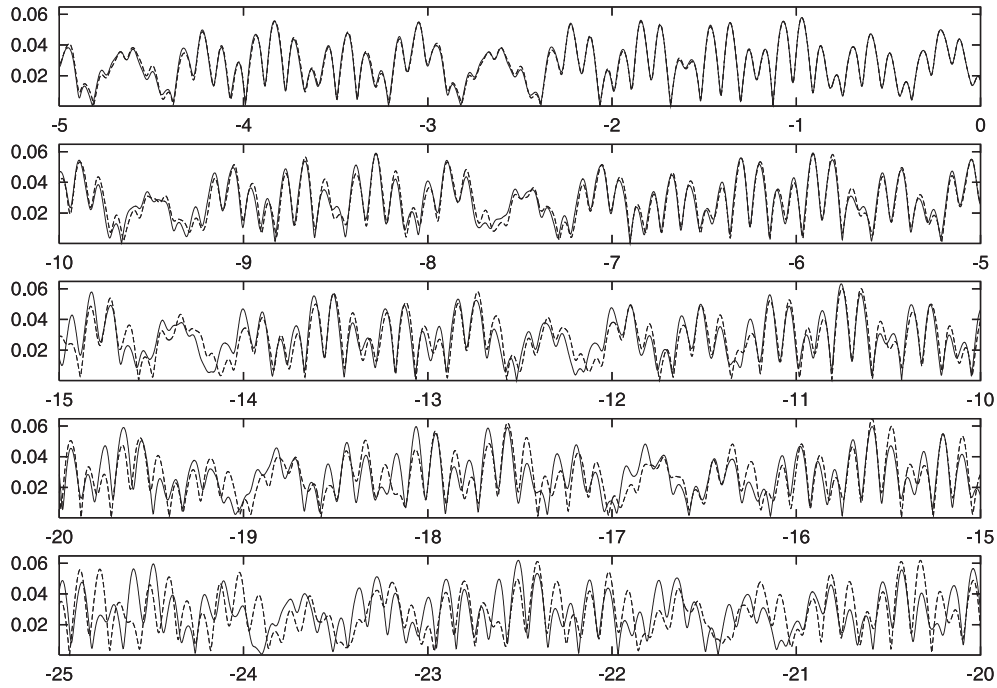


**Fig. 5.** Eccentricity of the Earth over 25 Myr in negative time from J2000. The solid line stands for the present solution La2004, while the dotted line is the eccentricity in the La93 solution (Laskar et al. 1993). The differences of the two solutions becomes noticeable after 10 Myr, and significantly different after 15–20 Myr.

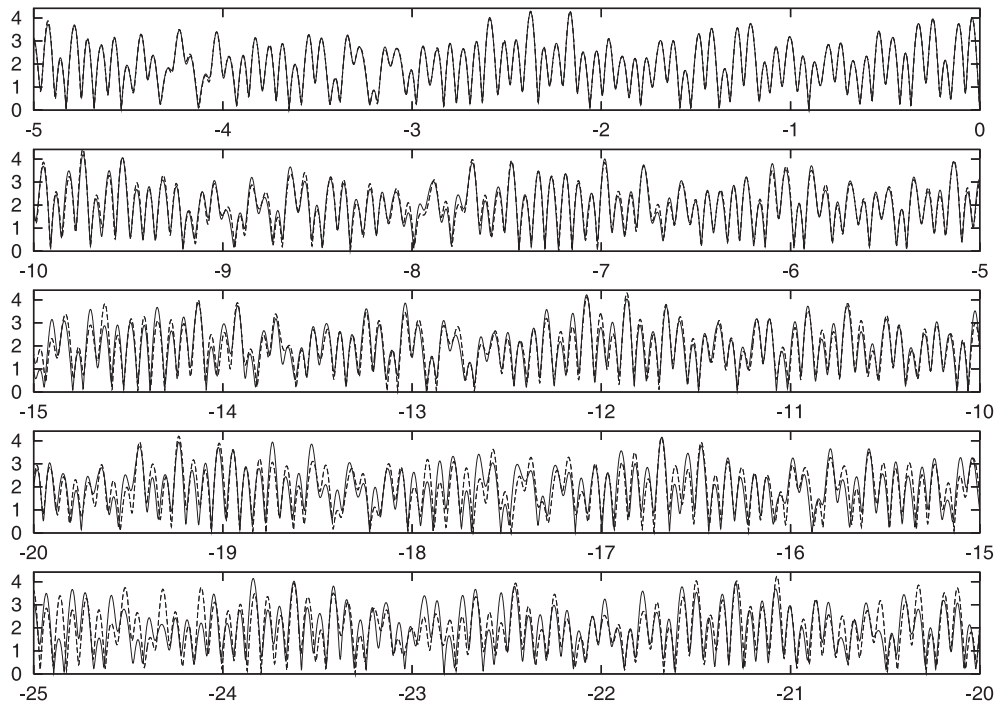


**Fig. 6.** Inclination (in degrees) of the Earth with respect to the fixed ecliptic J2000 over 25 Myr in negative time from J2000. The solid line stands for the present solution La2004, while the dotted line is the eccentricity in the La93 solution (Laskar et al. 1993). The differences of the two solutions become noticeable after 15 Myr, and significantly different after 20 Myr.

has only very small variations (Fig. 11). Indeed, as shown by Laplace (1773) and Lagrange (1776), there are no secular variations of the semi-major axis of the planets at first order with respect to the masses, while some terms of higher order can be present (Haretu 1885). These terms are very small for the

inner planets, but more visible in the solutions of the outer planets where the proximity of some mean motion resonances increases their contribution at second order with respect to the masses (Milani et al. 1987; Bretagnon & Simon 1990). For the solution of the Earth, they are so small that they will not induce

**Table 3.** Main secular frequencies  $g_i$  and  $s_i$  of La2004 determined over 20 Ma for the four inner planets, and over 50 Ma for the 5 outer planets (in arcsec yr<sup>-1</sup>).  $\Delta_{100}$  and  $\Delta_{250}$  are the observed variations of the frequencies over respectively 100 and 250 Myr. In the last column, the period of the secular term are given.

	(''/yr)	$\Delta_{100}$	$\Delta_{250}$	Period (yr)
$g_1$	5.59	0.13	0.20	231 843
$g_2$	7.452	0.019	0.023	173 913
$g_3$	17.368	0.20	0.20	74 620
$g_4$	17.916	0.20	0.20	72 338
$g_5$	4.257452	0.000030	0.000030	304 407
$g_6$	28.2450	0.0010	0.0010	45 884
$g_7$	3.087951	0.000034	0.000048	419 696
$g_8$	0.673021	0.000015	0.000021	1 925 646
$g_9$	-0.34994	0.00063	0.0012	3 703 492
$s_1$	-5.59	0.15	0.16	231 843
$s_2$	-7.05	0.19	0.25	183 830
$s_3$	-18.850	0.066	0.11	68 753
$s_4$	-17.755	0.064	0.14	72 994
$s_5$	0.00000013	0.0000001	0.0000001	
$s_6$	-26.347855	0.000076	0.000087	49 188
$s_7$	-2.9925259	0.000025	0.000025	433 079
$s_8$	-0.691736	0.000010	0.000011	1 873 547
$s_9$	-0.34998	0.00051	0.0011	3 703 069

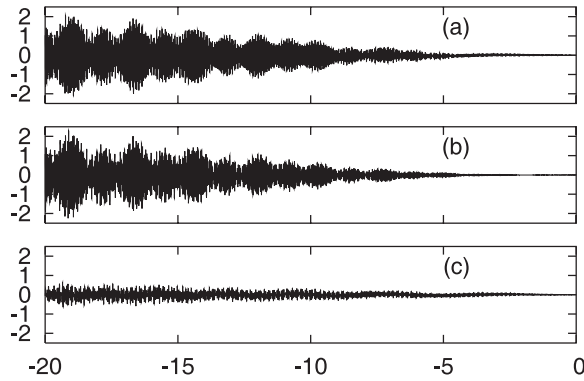


**Fig. 7.** Differences in obliquity (in degrees) La2004–La93(1, 1) versus time (in Myr) over 20 Myr from present **a**). In La2004 both orbital and precession models have been changed. In **b**) only the precession model has been changed, while in **c**) only the orbital motion has been changed. It is thus clear that the main change in La2004 arise from the change of precession model.

any noticeable change of the mean Earth–Sun distance, or of the duration of the year in the geological past, at least over the past 250 millions of years.

It was first shown by Lagrange (1774, 1777) that the inclination and nodes of the planets suffer long term quasiperiodic variations. Shortly after, Laplace (1776) demonstrated that this was the same for the eccentricity and longitudes. Both computations were made using the linearization of the first order

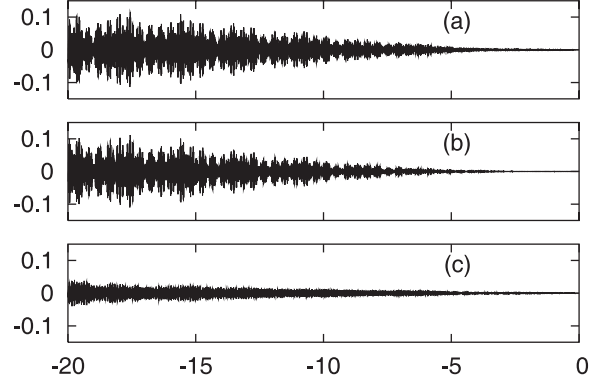


**Fig. 8.** Differences in climatic precession ( $e \sin \omega$ , where  $\omega = \varpi + \psi$  is the perihelion from the moving equinox) La2004–La93(1, 1) versus time (in Myr) over 20 Myr from present **a**). In La2004 both orbital and precession models have been changed. In **b**) only the precession model has been changed, while in **c**) only the orbital motion has been changed. It is thus clear that the main change in La2004 arise from the change of precession model.

averaged equations of motion. In this approximation, if we use the complex notations

$$z_k = e_k \exp(i\varpi_k); \quad \zeta_k = \sin(i_k/2) \exp(i\Omega_k), \quad (16)$$

the equations of motion are given by a linear equation

$$\frac{d[x]}{dt} = iA[x] \quad (17)$$

where  $[x]$  is the column vector  $(z_1, \dots, z_9, \zeta_1, \dots, \zeta_9)$ , and

$$A = \begin{pmatrix} A_1 & 0 \\ 0 & A_2 \end{pmatrix} \quad (18)$$

where the  $9 \times 9$  matrices (for 9 planets)  $A_1, A_2$  depend on the planetary masses and semi-major axis of the planets. The resolution of these equations is now classical, and is obtained through the diagonalization of the matrix  $A$  by the change of coordinates into proper modes  $u$

$$[x] = S[u]. \quad (19)$$

The solution in the proper modes  $[u] = (z_1^\bullet, \dots, z_9^\bullet, \zeta_1^\bullet, \dots, \zeta_9^\bullet)$  is then given by the diagonal system

$$\frac{d[u]}{dt} = iD[u] \quad (20)$$

where  $D = S^{-1}AS$  is a diagonal matrix  $D = \text{Diag}(g_1, g_2, \dots, g_9, s_1, s_2, \dots, s_9)$ , where all the eigenvalues  $g_k, s_k$  are real. The solutions of the proper modes  $z_k^\bullet, \zeta_k^\bullet$  are

$$z_k^\bullet(t) = z_k^\bullet(0) \exp(ig_k t); \quad \zeta_k^\bullet(t) = \zeta_k^\bullet(0) \exp(is_k t). \quad (21)$$

The solutions in the elliptical variables  $z_k, \zeta_k$  are then given as linear combinations of the proper modes (19), and becomes quasiperiodic functions of the time  $t$ , that is sums of pure periodic terms with independent frequencies.

$$z_k = \sum_{j=1}^9 \alpha_{kj} e^{ig_k t}; \quad \zeta_k = \sum_{j=1}^9 \beta_{kj} e^{is_k t}. \quad (22)$$

Lagrange (1781, 1782) actually did this computation for a planetary system including Mercury, Venus, Earth, Mars, Jupiter and Saturn. Pontécoulant (1834) extended it to the 7 known planets of the time, but with several errors in the numerical constants. The first precise solution for the Earth was given by Le Verrier (1856) for 7 planets, and was later on extended by Stockwell (1873) with the addition of Neptune. The validity of the linear approximation (17) was also questioned and subsequent improvements introduced some additional contribution of higher degree in eccentricity and inclination in Eq. (17), as well as terms of higher order with respect to the planetary masses in the averaged equations (Hill 1897; Brouwer & Van Woerkom 1950; Bretagnon 1974; Duriez 1977; Laskar 1985). With the addition of additional non linear terms  $B(x, \bar{x})$  (of degree  $\geq 3$  in eccentricity and inclination), the secular equations

$$\frac{d[x]}{dt} = iA[x] + B(x, \bar{x}) \quad (23)$$

are no longer integrable. Nevertheless, one can formally perform a Birkhoff normalization of Eq. (23) and after truncation, obtain some quasiperiodic expressions

$$\begin{aligned} z_j^*(t) &= \sum_{k=1}^9 a_{jk} e^{ig_k t} + \sum_{(k)} a_{j(k)} e^{i\langle(k), \nu \rangle t} \\ \zeta_j^*(t) &= \sum_{k=1}^9 b_{jk} e^{is_k t} + \sum_{(k)} b_{j(k)} e^{i\langle(k), \nu \rangle t} \end{aligned} \quad (24)$$

where  $(k) = (k_1, \dots, k_{18}) \in \mathbb{Z}^{18}$ ,  $\nu = (g_1, \dots, g_9, s_1, \dots, s_9)$ , and  $\langle(k), \nu \rangle = k_1 g_1 + \dots + k_9 g_9 + k_{10} s_1 + \dots + k_{18} s_9$ . The quasiperiodic expressions  $z_j^*(t), \zeta_j^*(t)$ , have been computed at various orders and degrees in eccentricity and inclination of expansion (Hill 1897; Bretagnon 1974; Duriez 1977; Laskar 1984, 1985), but as forecasted by Poincaré (1893), it was found that when all the main planets are taken into account, these formal expansions do not converge (Laskar 1984), for initial conditions close to the initial conditions of the Solar System, even at the lowest orders, and thus will not provide good approximation of the Solar System motion over very long time. In other terms, it appears that the actual solution of the Solar System is not close to a KAM tori (see Arnold et al. 1988) of quasiperiodic solutions.

Over a finite time of a few millions of years, one can still numerically integrate the equation of motion, and then search through frequency analysis (Laskar 1990, 1999, 2003) for a quasiperiodic approximation of the solution of the form (23). The non regular behavior of the solution will induce a drift of the frequencies in time, related to the chaotic diffusion of the trajectories (Laskar 1990, 1993, 1999).

In Table 3, the fundamental frequencies of the solution La2004 have been computed by frequency analysis over 20 Myr of the proper modes  $(z_1^*, \dots, z_4^*, \zeta_1^*, \dots, \zeta_4^*)$  related to the inner planets (Mercury, Venus, Earth, Mars), and over 50 Myr for the proper modes  $(z_5^*, \dots, z_9^*, \zeta_5^*, \dots, \zeta_9^*)$  associated to the outer planets (Jupiter, Saturn, Uranus, Neptune, Pluto) (Table 3). This difference reflects the fact that the main

source of chaotic behavior comes from overlap of secular resonances in the inner planet system, and that the outer planets secular systems is more regular than the inner one. Actually, in Cols. 2 and 3 of Table 3, we give the maximum observed in the variation of the secular frequencies over 100 and 250 Myr, in both positive and negative time, for our nominal solution La2004. These figures are in very good agreement with the equivalent quantities given in Table X of (Laskar 1990) for the integration of the secular equations. The number of digits of the fundamental frequencies in Table 3 is different for each frequency and reflects the stability of the considered frequency with time. Additionally, we have given in Figs. 9 and 10 the actual evolution of the secular frequencies obtained with a sliding window with a step size of 1 Myr (compare to Laskar 1990, Figs. 8 and 9).

## 8. Analytical approximations

### 8.1. Orbital motion

It is interesting for practical use to have an analytical expression for the main orbital quantities of the Earth. From the numerical values of La2004, we have performed a frequency analysis (Laskar 1990, 1999, 2003) in order to obtain a quasiperiodic approximation of the solutions over a few Myr. In order to be consistent with the remaining part of the paper, we chose a time interval covering 20 Myr. As we are mostly interested over negative time, we made the analysis from  $-15$  Myr to  $+5$  Myr, as usually, the precision of the approximation decreases at the edges of the time interval. The analysis of the eccentricity variables  $z = e \exp i\varpi$  is given in Table 4.  $z$  is obtained as

$$z = \sum_{k=1}^{26} b_k e^{i(\mu_k t + \varphi_k)}. \quad (25)$$

It should be noted that in the present complex form, the approximation is much more precise than what would give an equivalent quasiperiodic approximation of the eccentricity. Even with twice the number of periodic terms, the direct approximation of the eccentricity is not as good as the approximation obtained in complex variables. Moreover, here we obtain at the same time the approximation of the longitude of perihelion of the Earth from the fixed J2000 equinox ( $\varpi$ ). The comparison of this approximation, limited to only 26 terms, to the actual solution for the eccentricity of the Earth, is plotted in Fig. 12 (top).

Nevertheless, for information, we will give also here the leading terms in the expansion of the eccentricity as they may be useful in paleoclimate studies (Table 6). The three leading terms in eccentricity are well known in paleoclimate studies  $g_2 - g_5$  (405 kyr period),  $g_4 - g_5$  (95 kyr period), and  $g_4 - g_2$  (124 kyr period).

The solution for the inclination variables  $\zeta = \sin i/2 \exp i\Omega$  where  $i, \Omega$  are the Earth inclination and longitude of node with respect to the fixed ecliptic and equinox J2000, limited to 24 quasiperiodic terms

$$\zeta = \sum_{k=1}^{24} a_k e^{i(\nu_k t + \phi_k)}, \quad (26)$$

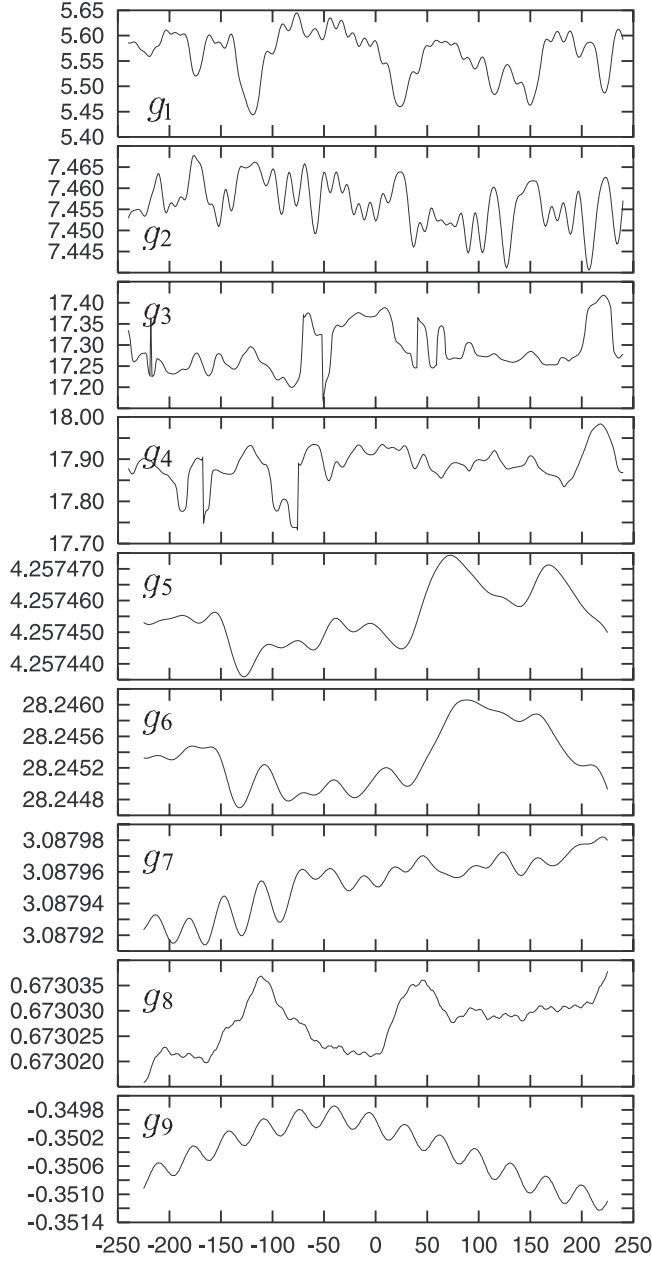


**Fig. 9.** Variation of the secular frequencies  $g_{1-9}$  from  $-250$  to  $+250$  Myr. The frequencies are computed over 20 Myr for  $g_{1-4}$  and over 50 Myr for  $g_{5-9}$ , after transformation of elliptical elements to proper modes (Laskar 1990).

is given in Table 5. The comparison of this quasiperiodic approximation with the complete solution is given in Fig. 12 (bottom). It should be noted that in Table 5, the first 22 terms are the terms of largest amplitude in the frequency decomposition of the inclination variable  $\zeta$ , but the two last terms, of frequency  $\nu_{23}$  and  $\nu_{24}$  are of much smaller amplitude. They have been kept in the solution, as they are close to the resonance with the main precession frequency.

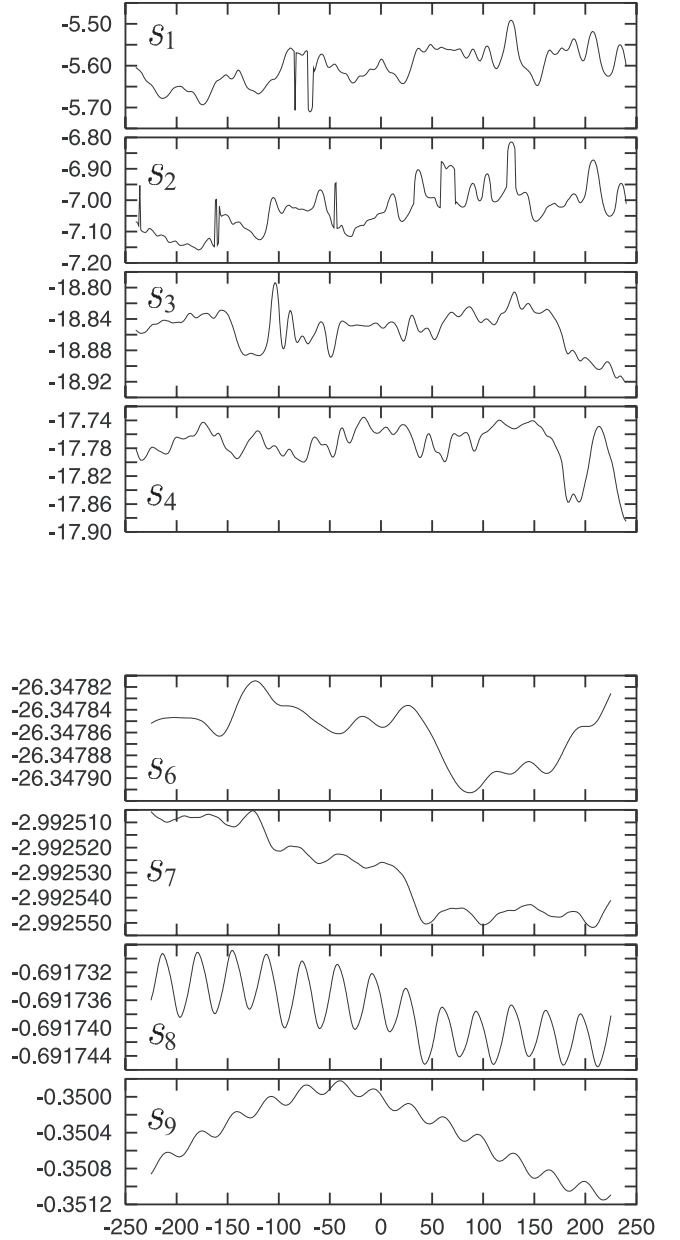


**Fig. 10.** Variation of the secular frequencies  $s_{1-9}$  from  $-250$  to  $+250$  Myr. The frequencies are computed over 20 Myr for  $s_{1-4}$  and over 50 Myr for  $s_{6-9}$ , after transformation of elliptical elements to proper modes (Laskar 1990).

## 8.2. Obliquity and precession

The solutions for precession and obliquity are obtained through the precession Eq. (6). In absence of planetary perturbations, the obliquity is constant ( $\varepsilon = \varepsilon_0$ ), and

$$\frac{d\psi}{dt} = \alpha \cos \varepsilon_0. \quad (27)$$

We have thus  $\psi = \psi_0 + p t$  where  $p = \alpha \cos \varepsilon_0$  is the precession frequency. This can be considered as a solution of order zero.

**Table 4.** Frequency decomposition of  $z = e \exp i\varpi$  for the Earth on the time interval  $[-15, +5]$  Myr (Eq. (25)).

$n$		$\mu_k$ (″/yr)	$b_k$	$\varphi_k$ (degree)
1	$g_5$	4.257564	0.018986	30.739
2	$g_2$	7.456665	0.016354	−157.801
3	$g_4$	17.910194	0.013055	140.577
4	$g_3$	17.366595	0.008849	−55.885
5	$g_1$	5.579378	0.004248	77.107
6		17.112064	0.002742	47.965
7		17.654560	0.002386	61.025
8		6.954694	0.001796	−159.137
9	$2g_3 - g_4$	16.822731	0.001908	105.698
10	$g_6$	28.244959	0.001496	127.609
11		18.452681	0.001325	156.113
12		5.446730	0.001266	−124.155
13		18.203535	0.001165	−92.112
14		7.325741	0.001304	−175.144
15		7.060100	0.001071	2.423
16		7.587926	0.000970	34.169
17		5.723726	0.001002	112.564
18		16.564805	0.000936	24.637
19		16.278532	0.000781	−90.999
20		18.999613	0.000687	0.777
21		3.087424	0.000575	120.376
22		17.223297	0.000577	−113.456
23		6.778196	0.000651	117.184
24		6.032715	0.000416	174.987
25		6.878659	0.000497	95.424
26		5.315656	0.000392	33.255

If we keep only the terms of degree one in inclination in Eqs. (6), we obtain the solution of order one

$$\frac{d\varepsilon}{dt} = 2(\dot{p} \sin \psi - \dot{q} \cos \psi) = 2\operatorname{Re}(\dot{\zeta} e^{i\psi}). \quad (28)$$

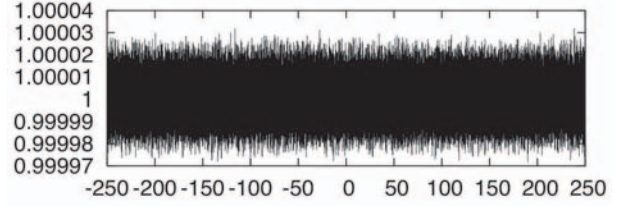
With the quasiperiodic approximation

$$\zeta = \sum_{k=1}^N a_k e^{i(\nu_k t + \phi_k)}, \quad (29)$$

of Table 5, the first order solution in obliquity will be a similar quasiperiodic function

$$\varepsilon = \varepsilon_0 + 2 \sum_{k=1}^N \frac{a_k \nu_k}{\nu_k + p} \cos((\nu_k + p)t + \phi_k + \psi_0), \quad (30)$$

with a similar form for the solution of precession  $\psi$ . This first order approximation will only be valid when we are far from resonance, that is  $|\nu_k + p| \gg 0$ . This is not the case for the last term  $\nu_{23} = s_6 + g_5 - g_6 = -50.336259$  arcsec yr<sup>−1</sup> in Table 5, as  $p \approx 50.484$  arcsec yr<sup>−1</sup>. This resonant term can lead to a

**Fig. 11.** Variation of the semi-major axis of the Earth–Moon barycenter (in AU) from  $-250$  to  $+250$  Myr.**Table 5.** Frequency decomposition of  $\zeta = \sin i/2 \exp i\Omega$  for the Earth on the time interval  $[-15, +5]$  Myr (Eq. (26)).

$n$		$\nu_k$ (″/yr)	$a_k$	$\phi_k$ (degree)
1	$s_5$	−0.000001	0.01377449	107.581
2	$s_3$	−18.845166	0.00870353	−111.310
3	$s_1$	−5.605919	0.00479813	4.427
4	$s_2$	−7.050665	0.00350477	130.826
5	$s_4$	−17.758310	0.00401601	−77.666
6		−18.300842	0.00262820	−93.287
7		−7.178497	0.00189297	−65.292
8		−6.940312	0.00164641	−66.106
9		−6.817771	0.00155131	−46.436
10		−19.389947	0.00144918	50.158
11		−5.481324	0.00154505	23.486
12	$s_6$	−26.347880	0.00133215	127.306
13		−19.111118	0.00097602	159.658
14		−2.992612	0.00088810	140.098
15		−6.679492	0.00079348	−43.800
16		−5.835373	0.00073058	−160.927
17		−0.691879	0.00064133	23.649
18		−6.125755	0.00049598	143.759
19		−5.684257	0.00054320	138.236
20		−18.976417	0.00040739	−105.209
21		−7.290771	0.00041850	106.192
22		−5.189414	0.00033868	50.827
23	$s_6 + g_5 - g_6$	−50.336259	0.00000206	−150.693
24		−47.144010	0.00000023	−167.522

significant change in the obliquity variations, and have been studied in detail in Laskar et al. (1993).

Another difficulty, arising with the obliquity solution, is due to the dissipation in the Earth–Moon system, which induces a significant variation of the precession frequency with time, as the Earth rotation  $\omega$  slows down, and the Earth–Moon distance  $a_M$  increases.

We have plotted in Fig. 14 the evolution of the obliquity of the Earth from  $-250$  to  $+250$  Myr. The effect of the tidal dissipation is clearly visible on this timescale, and there is a general increase of the obliquity from  $-250$  Myr to present time. In positive time, there is an obvious singularity in the obliquity, with a decrease of about 0.4 degree. This results from the



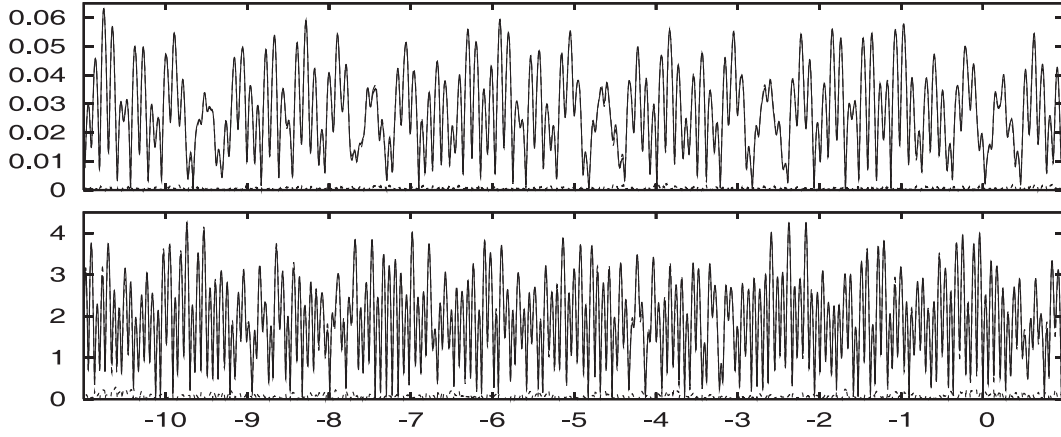


**Fig. 12.** (Top) Eccentricity of the Earth from  $-11$  to  $+1$  Myr. The solid curve is the solution La2004. Almost completely hidden behind the solid curve is a dashed curve representing the quasiperiodic approximation of Table 4 with 26 periodic terms. (Bottom) Inclination of the Earth from  $-11$  to  $+1$  Myr. The solid curve is the solution La2004. The dashed line (almost identical to the solid curve) is the quasiperiodic approximation of Table 5 with 24 periodic terms. On both plots, as the two curves are nearly identical, the difference of the two solutions is also plotted in dotted curve.

crossing of the resonance with the term  $s_6 + g_5 - g_6$  that was already described in a different context in Laskar et al. (1993). After this sudden decrease, the obliquity increases again, with roughly the same trend. An additional (but smaller singularity is observable around  $+150$  Myr, that corresponds to the crossing of the resonance with the term  $\nu_{24}$  (Table 5). The averaged obliquity can be well approximated in negative time with the expression

$$\varepsilon_M = 23.270773 + 2.011295 T \quad (31)$$

where  $\varepsilon_M$  is in degree, and  $T$  in billion of years (Gyr). In the interval  $[+20 \text{ Myr}, +130 \text{ Myr}]$  this approximation becomes

$$\varepsilon_M = 22.893171 + 1.952715 T \quad (32)$$

so the main effect of the crossing of the resonance is a decrease of  $0.377602$  degree of the obliquity. This effect can be easily understood with the analytical integration of a simple model, in terms of Fresnel integrals (see Appendix A).

### 8.3. Approximation for the obliquity

As for the solutions of the orbital elements, we have obtained an approximation formula for the evolution of the obliquity of the Earth over the period from  $-15$  Myr to  $+5$  Myr. Obtaining this solution presents some additional difficulties because of the dissipative effects in the Earth–Moon system that induces a significative change of the precession frequency. The obliquity is obtained on the form

$$\varepsilon = \varepsilon_0 + \sum_{k=1}^N a'_k \cos((\nu'_k + p_1 t) t + \phi'_k), \quad (33)$$

where  $\varepsilon_0 = 23.254500$  degrees, and the coefficients  $a'_k, \nu'_k, \phi'_k$  are given in Table 7. The coefficient  $p_1$  (Eq. (35)) results from the secular change of the precession frequency (34) due to tidal dissipation (see next).

The comparison with the full solution is given in Fig. 15, over selected periods of time, from  $-11$  Myr to the present.

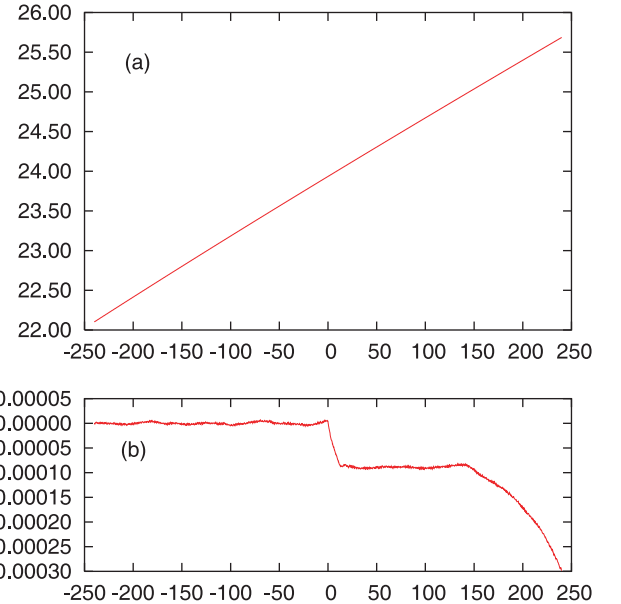


**Fig. 13.** **a)** Evolution of length of the day for the Earth, in hours, from  $-250$  to  $+250$  Myr. **b)** Residuals with the fit of the averaged solution with the polynomial expression (41).

In Table 7, the terms of frequency  $\nu'_k$  are recognized as combinations of the form  $p + \nu_k$ , where  $p$  is the precession frequency, and  $\nu_k$  a secular frequency from the secular motion of the orbital plane (from Table 5). The approximation is made over the interval  $[-15 \text{ Myr}, +2 \text{ Myr}]$  with  $p = p_0 + p_1 T$ , where  $p_0$  and  $p_1$  are taken from Eq. (35).

### 8.4. Approximation for the precession

The full approximate solution for the precession is more complicated because of the presence of the secular resonance  $s_6 + g_5 - g_6$ . In fact, the proximity of this resonance is responsible for the largest periodic term in the expression of the precession



**Table 6.** Frequency decomposition of the eccentricity of the Earth on the time interval  $[-15, +5]$  Myr. For all computations, the data of Table 4 should be preferred. Here,  $e = e_0 + \sum_{k=1}^{20} b'_k \cos(\mu'_k t + \varphi_k)$  with  $e_0 = 0.0275579$ . For each term, in the first column is the corresponding combination of frequencies where  $g_i$  are the fundamental frequencies (Table 3), and  $\mu_j$  the frequencies of the terms in  $z$  from Table 4.

$k$		$\mu'_k$ ("/yr)	$P$ (yr)	$b'_k$	$\varphi'_k$ (degree)
1	$g_2 - g_5$	3.199279	405 091	0.010739	170.739
2	$g_4 - g_5$	13.651920	94 932	0.008147	109.891
3	$g_4 - g_2$	10.456224	123 945	0.006222	-60.044
4	$g_3 - g_5$	13.109803	98 857	0.005287	-86.140
5	$g_3 - g_2$	9.909679	130 781	0.004492	100.224
6	$\mu_7 - \mu_6$	0.546076	2 373 298	0.002967	-168.784
7	$g_1 - g_5$	1.325696	977 600	0.002818	57.718
8	$g_4 - g_1$	12.325286	105 150	0.002050	49.546
9	$g_2 - g_5 + \mu_6 - \mu_7$	2.665308	486 248	0.001971	148.774
10	$g_2 - g_1$	1.883616	688 038	0.001797	137.155
11	$\mu_6 - g_5$	12.856520	100 805	0.002074	24.487
12	$g_2 + g_4 - 2g_5$	16.851127	76 909	0.001525	102.380
13	$\mu_6 - g_2$	9.650041	134 300	0.001491	-167.676
14	$2g_3 - g_4 - g_5$	12.563233	103 158	0.001316	69.234
15	$2g_4 - g_2 - g_3$	10.975914	118 077	0.001309	-51.163
16	$g_1 - g_3$	11.788709	109 936	0.001300	-146.081
17	$\mu_7 - g_2$	10.194846	127 123	0.001306	-139.827
18	$g_3 + g_4 - g_2 - g_5$	23.562689	55 002	0.001261	30.098
19	$\mu_7 - g_5$	13.398519	96 727	0.001344	27.612
20	$g_2 + g_4 - g_3 - g_5$	3.742221	346 318	0.001058	178.662

angle (Fig. 16). The precession angle can thus be approximate by ( $\psi$  in arcsec,  $t$  in years)

$$\psi = +49086 + p_0 t + p_1 t^2 + 42246 \frac{\nu_0^2}{(\nu_0 + 2p_1 t)^2} \cos(\nu_0 t + p_1 t^2 + \phi_0) \quad (34)$$

where

$$\begin{aligned} \nu_0 &= 0.150019''/\text{yr} \\ p_0 &= 50.467718''/\text{yr} \\ p_1 &= -13.526564^{-9}''/\text{yr}^2 \\ \phi_0 &= 171.424 \text{ degree}. \end{aligned} \quad (35)$$

It should be noted that in this formula, the cosine term is an approximation for a more complicated expression that arises from a double integration of the term  $\cos(\nu_0 t + p_1 t^2 + \phi_0)$  in the expression of the derivative of the obliquity (6). In order to obtain an expression as simple as possible, without expressions involving Fresnel integrals (Appendix A), we had to restrain its interval of validity to  $[-15, +2]$  Myr.

For paleoclimate studies, the usual quantity that relates more directly to insolation is the climatic precession  $e \sin \bar{\omega}$ , where  $\bar{\omega} = \psi + \varpi$  is the longitude of the perihelion from the moving equinox. We have thus

$$e \sin \bar{\omega} = \Im(z e^{i\psi(t)}), \quad (36)$$

where the decomposition of  $z = e \exp(i\varpi)$  is provided in Table 4, and the precession angle  $\psi$  is given by Eq. (34).

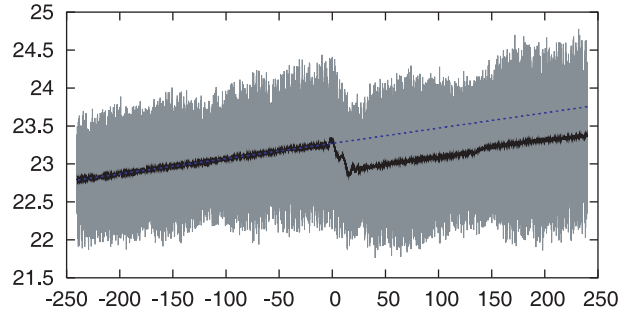


**Fig. 14.** Evolution of the obliquity of the Earth in degrees, from  $-250$  to  $+250$  Myr. The grey zone is the actual obliquity, while the black curve is the averaged value of the obliquity over  $0.5$  Myr time intervals. The dotted line is a straight line fitted to the average obliquity in the past.

The comparison of this approximation with the complete solution from  $-11$  to  $+1$  Myr is given in Fig. 17. The solution for climatic precession is thus on the form

$$e \sin \bar{\omega} = \sum_{k=1}^{20} b_k \sin(\mu_k t + \varphi_k + \psi(t)), \quad (37)$$

where  $b_k, \mu_k, \varphi_k$  are from Table 4, and where  $\psi(t)$  is given by Eq. (34). The frequencies of the terms of the climatic precession are thus of the form

$$\mu'_k = \mu_k + p + p_1 t, \quad (38)$$

where  $p, p_1$  are given in Eqs. (34) and (35).

**Table 7.** Approximation for the obliquity of the Earth, following Eq. (33). This expression is not strictly quasiperiodic, because of the presence of the dissipative term  $p_1$  in the evolution of the precession frequency (33).

$k$		$\nu'_k$ ("/yr)	$P$ (yr)	$a'_k$	$\phi'_k$ (d)
1	$p + s_3$	31.626665	40 978	0.582412	86.645
2	$p + s_4$	32.713667	39 616	0.242559	120.859
3	$p + s_6$	24.124241	53 722	0.163685	-35.947
4	$p + \nu_6$	32.170778	40 285	0.164787	104.689
5	$p + \nu_{10}$	31.081475	41 697	0.095382	-112.872
6	$p + \nu_{20}$	31.493347	41 152	0.094379	60.778
7	$p + s_6 + g_5 - g_6$	0.135393	9 572 151	0.087136	39.928
8	$p + s_2$	43.428193	29 842	0.064348	-15.130
9	$p + s_1$	44.865444	28 886	0.072451	-155.175
10		31.756641	40 810	0.080146	-70.983
11	$p + \nu_{13}$	31.365950	41 319	0.072919	10.533
12		32.839446	39 465	0.033666	-31.614
13		32.576100	39 784	0.033722	77.554
14		32.035200	40 455	0.030677	71.757
15	$p + \nu_8$	43.537092	29 768	0.039351	145.835
16	$p + \nu_7$	43.307432	29 926	0.030375	160.109
17	$p + \nu_9$	43.650496	29 690	0.024733	144.926
18		31.903983	40 622	0.025201	-173.656
19		30.945195	41 880	0.021615	-144.933
20		23.986877	54 030	0.021565	-79.670
21		24.257837	53 426	0.021270	-178.441
22		32.312463	40 108	0.021851	-24.566
23		44.693687	28 997	0.014725	124.744

### 8.5. Earth–Moon system

In Fig. 18, the evolution of the Earth–Moon semi-major  $a_M$  axis is plotted over 250 Myr in positive and negative time. The grey area corresponds to the short period variations of the Earth–Moon distance, obtained in the full integration of the system, while the black curve is the integration of the averaged equations that is used for the precession computations. The agreement between the two solutions is very satisfying.

We have searched for a polynomial approximation for the secular evolution of  $a_M$ , in order to provide a useful formula for simple analytical computations. In fact, the Earth–Moon evolution is driven by the tidal dissipation equations (Sect. 4.1), that involve the obliquity of the planet. The important singularity of the obliquity in the future (see previous section) prevents from using a single approximation over the whole time interval, and we have used a different polynomial in positive and negative time.

$$\begin{aligned}
 a_M^- &= 60.142611 & a_M^+ &= 60.142611 \\
 &+ 6.100887 T & &+ 6.120902 T \\
 &- 2.709407 T^2 & &- 2.727887 T^2 \\
 &+ 1.366779 T^3 & &+ 1.614481 T^3 \\
 &- 1.484062 T^4 & &- 0.926406 T^4
 \end{aligned} \quad (39)$$

where  $T$  is in billions of years (Gyr), and  $a_M^{\pm}$  in Earth radius (see Table 1). In the residuals plot (Fig. 18b), we can check that this polynomial approximation is very precise for negative time, but in positive time, we have an additional singularity around 150 Myr, resulting from the secular resonance of the precession frequency with  $\nu_{24}$  (Table 5).

In the same way, it is possible to approximate the evolution of the precession frequency of the Earth  $p$  as the Moon goes away and the rotation of the Earth slows down with time. The polynomial approximation of the precession frequency is then in  $\text{arcsec yr}^{-1}$ , with  $T$  in Gyr

$$\begin{aligned}
 p^- &= 50.475838 & p^+ &= 50.475838 \\
 &- 26.368583 T & &- 27.000654 T \\
 &+ 21.890862 T^2 & &+ 15.603265 T^2
 \end{aligned} \quad (40)$$

It should be said that the initial value is kept equal for both positive and negative time to avoid discontinuities. It is clear from Fig. 19 that for the period between +30 and +130 Myr, a better approximation could be obtained by adding to the constant part the offset  $+0.135052 \text{ arcsec yr}^{-1}$ . It is interesting to note again the dramatic influence of the resonance  $\nu_{23}$  on the

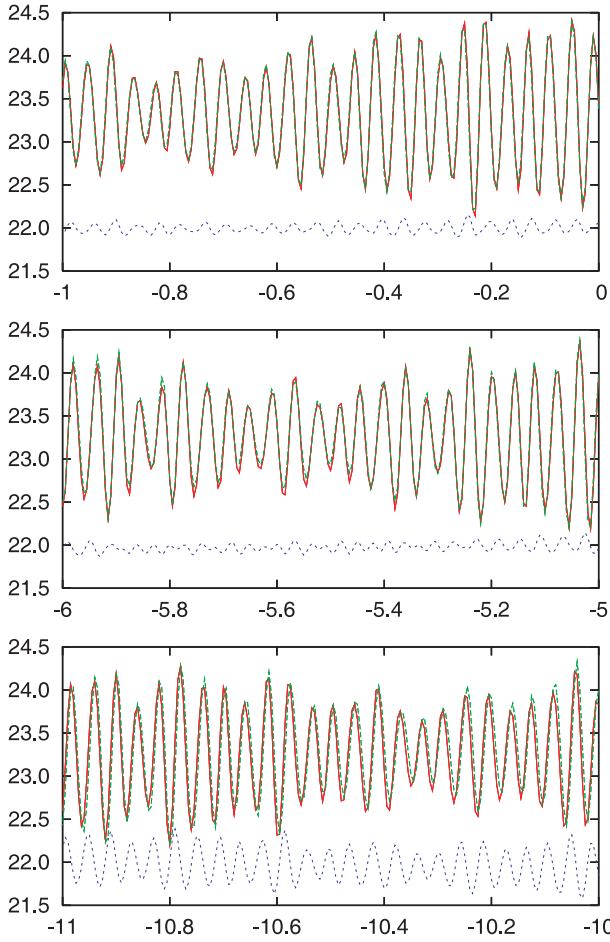


**Fig. 15.** Comparison of the solution of the obliquity La2004 (solid line) with its approximation using Table 7 (dotted line) with 26 periodic terms. The difference of two solutions (+22 degrees) is also plotted.

evolution of the precession frequency. The equivalent formulas for the length of the day are (in hours)

$$\begin{aligned}
 LOD^- &= 23.934468 & LOD^+ &= 23.934468 \\
 &+ 7.432167 T & &+ 7.444649 T \\
 &- 0.727046 T^2 & &- 0.715049 T^2 \\
 &+ 0.409572 T^3 & &+ 0.458097 T^3 \\
 &- 0.589692 T^4 & &
 \end{aligned} \quad (41)$$

One should note that Eqs. (39) and (41) correspond at the origin J2000 to a change in the semi major axis of the Moon of about 3.89 cm/yr, and a change of the LOD of 2.68 ms/century. These values slightly differ from the current ones of Dickey et al. (1994) ( $3.82 \pm 0.07$  cm/yr for the receding of the Moon). This is understandable, as the Earth–Moon model in our integration that was adjusted to DE406 is simplified with respect to the one of DE406.

## 9. Stability of the solution

In such long term numerical computations, the sources of errors are the error of method due to the limitation of the numerical integration algorithm, the numerical roundoff error resulting from the limitation of the representation of the real numbers

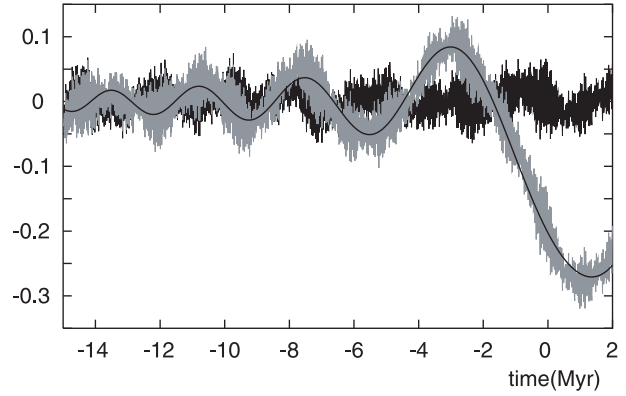


**Fig. 16.** Comparison of the solution of the precession La2004 with its approximation from  $-15$  to  $+2$  Myr. The grey curve is obtained after removing uniquely the secular trend  $\psi_0 + p_0 t + p_1 t^2$ . The dark curve are the residual (in radians) after removing the resonant term (Eq. (34)), which is also displayed in solid line.

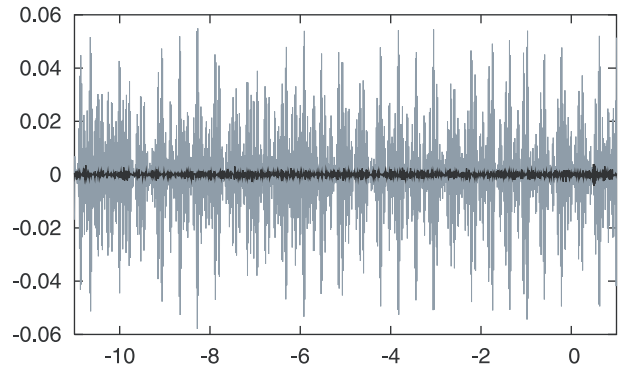


**Fig. 17.** Comparison of the solution of the climatic precession of La2004 with its approximation from  $-11$  to  $+1$  Myr. The grey curve is the full climatic precession  $e \sin \bar{\omega}$ . The dark curve are the residual after removing the approximation given by Eq. (37).

in the computer, and the errors of the initial conditions and of the model which are due to our imperfect knowledge of all the physical parameters in the Solar system, and to the necessary limitations of the model. Some of the main sources of uncertainty in the model for long term integrations were reviewed in (Laskar 1999). The effect of all these errors is amplified by the chaotic behaviour of the system, with an exponential increase of the difference between two solutions with different settings, until saturation due to the limited range of the considered variables. A summary of these limitations, extracted from (Laskar 1999) is given in Table 8, but it should be noted that these times of validity are probably pessimistic, as they correspond to analytical estimates based on the “worst case” situation. Our requirement for the precision of a long term solution is also not the same as for precise short term ephemeris. For the long term solutions, aimed at paleoclimate or qualitative studies, two solutions can be considered as similar, as long as the pattern of the two solutions (eccentricity for example), resulting (at first order) from the combination of various proper modes remain similar. This will last until some of the main proper modes get completely out of phase (see Sect. 7). It will be the same for the solutions in obliquity and precession.

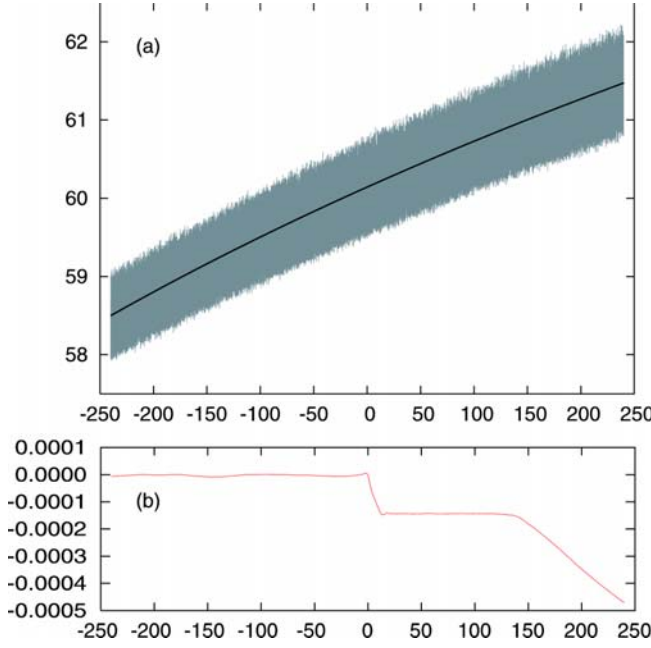


**Fig. 18.** **a)** Evolution of the Earth–Moon semi major axis (in Earth radii) from  $-250$  to  $+250$  Myr. The grey zone is the result of the integration of the full equations, while the black curve is the integration of the averaged equations, as used in the precession computations; **b)** residuals with the fit of the averaged solution with the polynomial expression (39).

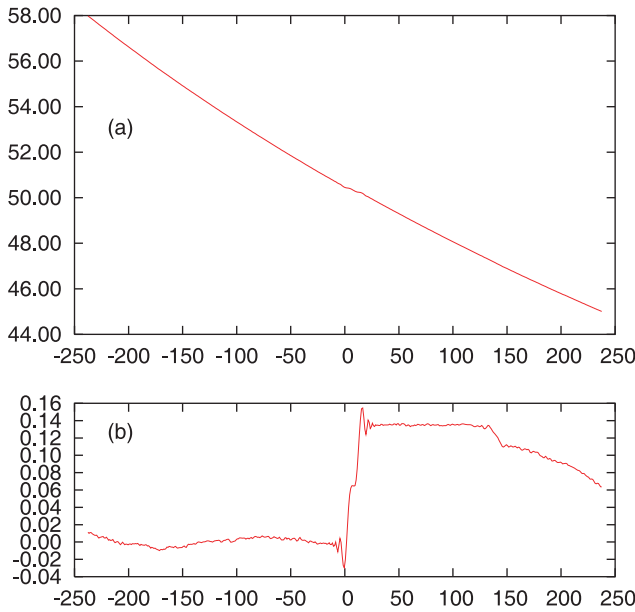


**Fig. 19.** **a)** Evolution of the precession frequency of the Earth  $p$  (in arcsec/yr)  $-250$  to  $+250$  Myr; **b)** residuals with the fit of the averaged solution with the polynomial expression (40).

### 9.1. Orbital motion

Practically, we have tested the stability of our solution by comparison of the eccentricity (Fig. 20) and inclination (Fig. 21) with different solutions. In Figs. 20a and 21a, the nominal solution La2004 (with stepsize  $\tau = 5 \times 10^{-3}$  years) is compared to an alternate solution, La2004\*, with the same dynamical

**Table 8.** Main sources of uncertainty in the orbital solution (from Laskar 1999). For each limiting factor, an analytical estimate of the time of validity of the solution  $T_V$  is given (in Myr), taking into account the exponential growth of the error.

Limiting factor	$T_V$
Uncertainty on the masses and initial conditions	38 Myr
Contribution of the main Galilean satellites	35 Myr
Uncertainty in the Earth–Moon system evolution	40 Myr
Effect of the main asteroids	32 Myr
Mass loss of the Sun	50 Myr
Uncertainty of $2 \times 10^{-7}$ on the $J_2$ of the Sun	26 Myr

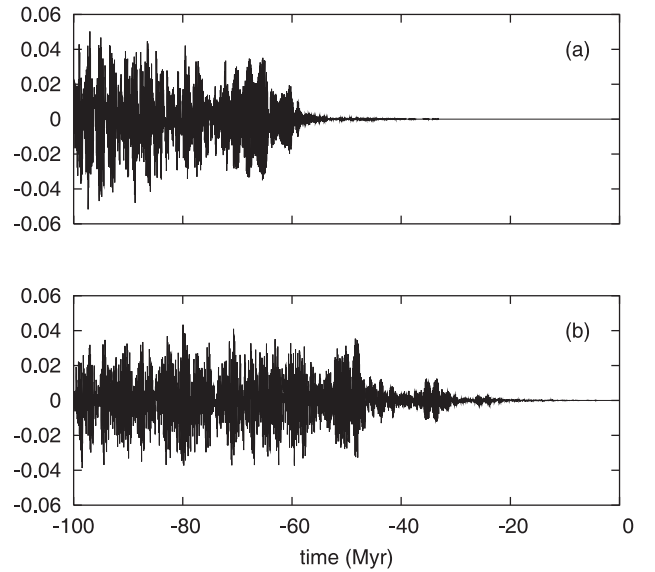


**Fig. 20.** Stability of the solution for eccentricity of the Earth. **a)** Difference of the nominal solution La2004 with stepsize  $\tau = 5 \times 10^{-3}$  years, and La2004\*, obtained with  $\tau^* = 4.8828125 \times 10^{-3}$  years; **b)** difference of the nominal solution with the solution obtained while setting  $J_2^S = 0$  for the Sun (instead of  $2 \times 10^{-7}$  in the nominal solution).

model, and a very close stepsize  $\tau^* = 4.8828125 \times 10^{-3}$  years (Table 9). This special value was chosen in order that our output time span  $h = 1000$  years corresponds to an integer number (204 800) of steps, in order to avoid any interpolation problems in the check of the numerical accuracy. This is thus a test of the time of validity for obtaining a precise numerical solution, resulting from method and roundoff errors of the integrator. It is thus limited here to about 60 Myr.

This limitation of 60 Myr is a limitation for the time of validity of an orbital solution, independently of the precision of the dynamical model. In order to go beyond this limit, the only way will be to increase the numerical accuracy of our computations, by improving the numerical algorithm, or with an extended precision for the number representation in the computer.

A second test is made on the uncertainty of the model. Several sources of uncertainty were listed in (Laskar 1999), and it was found that one of the main sources of uncertainty was due to the imprecise knowledge of the Solar

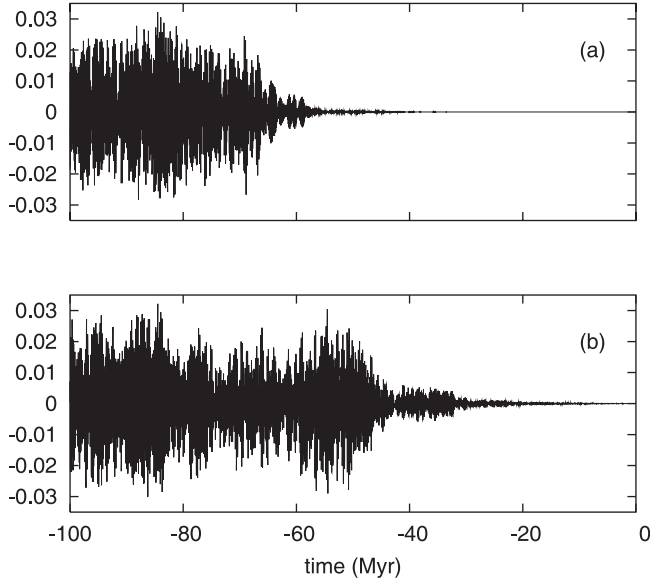


**Fig. 21.** Stability of the solution for inclination of the Earth. **a)** Difference of  $\sin i/2$  for the nominal solution La2004 with step-size  $\tau = 5. \times 10^{-3}$  years, and for La2004\*, obtained with  $\tau^* = 4.8828125 \times 10^{-3}$  years; **b)** difference of  $\sin i/2$  for the nominal solution with the solution obtained while setting  $J_2^S = 0$  for the Sun (instead of  $2 \times 10^{-7}$  in the nominal solution).

**Table 9.** Variants of the La2004 solutions. The nominal solution La2004 is obtained for a stepsize  $\tau = 5 \times 10^{-3}$ , and a Solar oblateness  $J_2^S = 2.0 \times 10^{-7}$ . The other solutions, with different setting have been computed to test the stability of the nominal solution. In the last column  $\gamma$  is the tidal dissipation factor.

Name	$\tau$ (yr)	$J_2^S$	$\gamma$
La2004	$5 \times 10^{-3}$	$2.0 \times 10^{-7}$	1
La2004*	$4.8828125 \times 10^{-3}$	$2.0 \times 10^{-7}$	1
La2004**	$5.00000005 \times 10^{-3}$	$2.0 \times 10^{-7}$	1
La2004 <sub>0</sub>	$5 \times 10^{-3}$	0	1
La2004 <sub>1.0</sub>	$5 \times 10^{-3}$	$1.0 \times 10^{-7}$	1
La2004 <sub>1.5</sub>	$5 \times 10^{-3}$	$1.5 \times 10^{-7}$	1
La2004 <sup>0.95</sup>	$5 \times 10^{-3}$	$2.0 \times 10^{-7}$	0.95
La2004 <sup>0.90</sup>	$5 \times 10^{-3}$	$2.0 \times 10^{-7}$	0.90

oblateness ( $J_2^S$ ) (Table 8). Its most recent determination, obtained with the SOHO and GONG helioseismic data give  $J_2^S = (2.18 \pm 0.06) \times 10^{-7}$  (Pijpers 1998), with a very similar value adopted in DE406 ( $J_2^S = 2 \times 10^{-7}$ , Standish 1998), while in DE200, it was not taken into account (Newhall et al. 1983). We will thus consider that comparing the nominal solution La2004 (with  $J_2^S = 2 \times 10^{-7}$ ) with an alternate solution (La2004<sub>0</sub>) with  $J_2^S = 0$  is representative of the uncertainty of the dynamical model for our long term integrations<sup>1</sup> (Table 9).

The results La2004 – La2004<sub>0</sub> for the Earth's eccentricity and inclination are displayed in (Figs. 20b and 21b)

<sup>1</sup> This empirical assumption is motivated by the fact that in Table 8, an error of  $2 \times 10^{-7}$  on  $J_2^S$  appear to be the largest limiting factor in the long term evolution of the solution.

over 100 Myr. As for Mars (Laskar et al. 2004), the effect of  $J_2^S$  becomes noticeable after about 30 Myr (26 Myr were predicted with an analytical estimate in (Laskar 1999), and the solution remains very similar over 40 Myr, and totally out of phase after 45 Myr. We will thus consider here that 40 Myr is about the time of validity of our present orbital solution for the Earth. Other integrations made with  $J_2^S = 1.5 \times 10^{-7}$  and  $J_2^S = 1.0 \times 10^{-7}$  (Table 9) gave practically the same estimates. It should be noted that with our present algorithms, we are much more limited by the precision of the model (Figs. 20b and 21b) than by the numerical accuracy (Figs. 20a and 21a).

## 9.2. Obliquity and precession

For the obliquity and precession, as was already mentioned in (Laskar et al. 1993), the main source of uncertainty is the evolution of the tidal dissipation and other related factors (see Sect. 4.1). Among these factors, one can mention the variations of the dynamical ellipticity of the Earth resulting from changes of the ice caps, or mantle convections. The maximal contribution of these effects can be estimated (see Levrard & Laskar 2003), but it is very difficult to obtain at present a precise value of their contributions. Moreover, the largest dissipative term, resulting from body tides can evolve substantially as a result of the variation of the distribution of the continents, as most of the tidal dissipation occurs in shallow seas (Jeffreys 1920, 1976; Egbert & Ray 2000).

In Fig. 22, we have explicited the result of a difference of 5% (Figs. 22a and c) and 10% (Figs. 22b and d) in the tidal dissipation term of the Earth and the Moon ( $\Delta t$  and  $\Delta t_M$  in Table 1). With 5% error (La2004<sup>(0.95)</sup>), the solution of obliquity is valid over about 20 Myr, but with a 10% error (La2004<sup>(0.90)</sup>), the solution is out of phase after 20 Myr. Nevertheless, the uncertainty in the tidal dissipation appears mostly as a small change of the precession frequency  $p$ , which reveals in the obliquity solution as a time offset that does not change much the obliquity pattern. Indeed, in Figs. 22e and f, we have made a readjustment of the time scale for the solutions La2004<sup>(0.95)</sup> and La2004<sup>(0.90)</sup> of respectively

$$\begin{aligned} \delta t_{(0.95)} &= 1.3346 \times 10^{-5} t - 1.9362 \times 10^{-5} t^2 \\ \delta t_{(0.90)} &= 1.4358 \times 10^{-5} t - 3.9666 \times 10^{-5} t^2 \end{aligned} \quad (42)$$

where  $t$  is in Myr. With this new time scales, the different solutions become very close over 40 Myr, that is over the full range of validity of the orbital solution (Figs. 22e and f). An uncertainty of 10% in the tidal dissipation term thus corresponds mostly to an uncertainty in the timescale of 16 kyr after 20 Myr, and 63 kyr after 40 Myr.

## 10. Resonant angles

### 10.1. Secular resonances

Using the secular equations, Laskar (1990, 1992), demonstrated that the chaotic behavior of the Solar system arises from multiple secular resonances in the inner solar system. In particular, the critical argument associated to

$$\theta = (s_4 - s_3) - 2(g_4 - g_3) \quad (43)$$



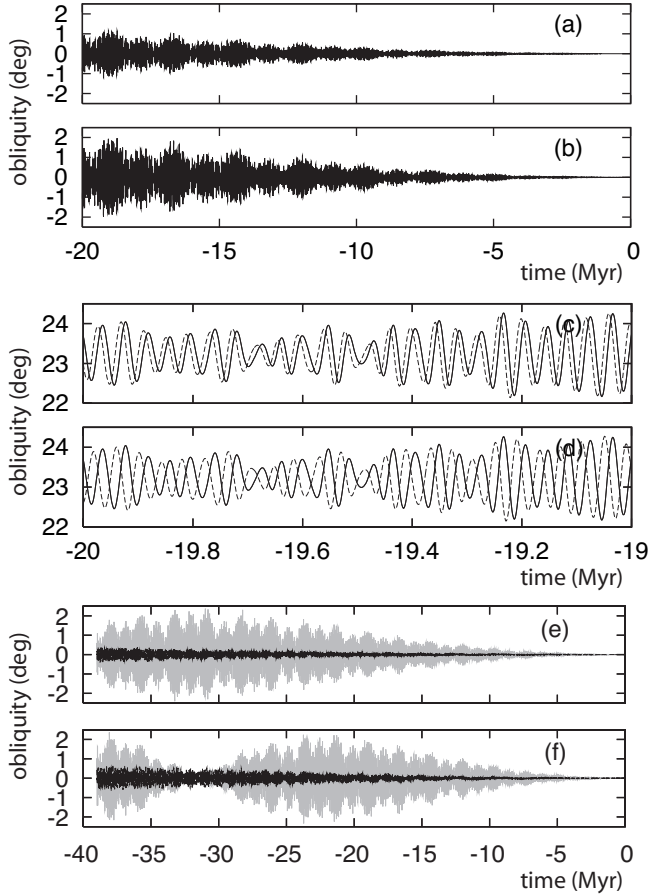


**Fig. 22.** Difference in obliquity for different tidal dissipation factor (Table 9): **a)**  $\text{La2004} - \text{La2004}^{(0.95)}$ ; **b)**  $\text{La2004} - \text{La2004}^{(0.90)}$ . In **c)** and **d)**, the nominal solution of the obliquity is plotted in solid line, while  $\text{La2004}^{(0.95)}$  **c)** and  $\text{La2004}^{(0.90)}$  **d)** are in dotted line. After an adjustment of the time scale, the differences of the solutions are much smaller over 40 Myr: **e)**  $\text{La2004} - \text{La2004}^{(0.95)}$ ; **f)**  $\text{La2004} - \text{La2004}^{(0.90)}$ .

where  $g_3, g_4$  are related to the precession of the perihelion of the Earth and Mars,  $s_3, s_4$  are related to the precession of the node of the same planets, is presently in a librational state, but can evolve in a rotational state, and even move to libration in a new resonance, namely

$$(s_4 - s_3) - (g_4 - g_3) = 0. \quad (44)$$

This reveals that a region of relatively strong instability results from the overlap (Chirikov 1979) of these two resonances. This result was questioned by Sussman & Wisdom (1992), as they did not recover such a large variation for the secular frequencies, but reached only  $2(s_4 - s_3) - 3(g_4 - g_3) = 0$  instead of Eq. (44). We have tested these resonant arguments in the nominal solution La2004, and in the alternate solutions La2004\*\*, La2004<sub>0</sub>, La2004<sub>1.5</sub> (Table 9).

In all variants of La2004 (Fig. 23 (top)), the resonant argument corresponding to  $\theta = (s_4 - s_3) - 2(g_4 - g_3)$  was in libration over the first 40 Myr, while the transition to circulation occurred at about 25 Myr in La93. All the solutions La2004, La2004\*\*, La2004<sub>0</sub>, La2004<sub>1.5</sub> differ significantly beyond 40 to 50 Myr, but they all enter the  $(s_4 - s_3) - (g_4 - g_3)$  resonance within 100 Myr, comforting the conclusions of

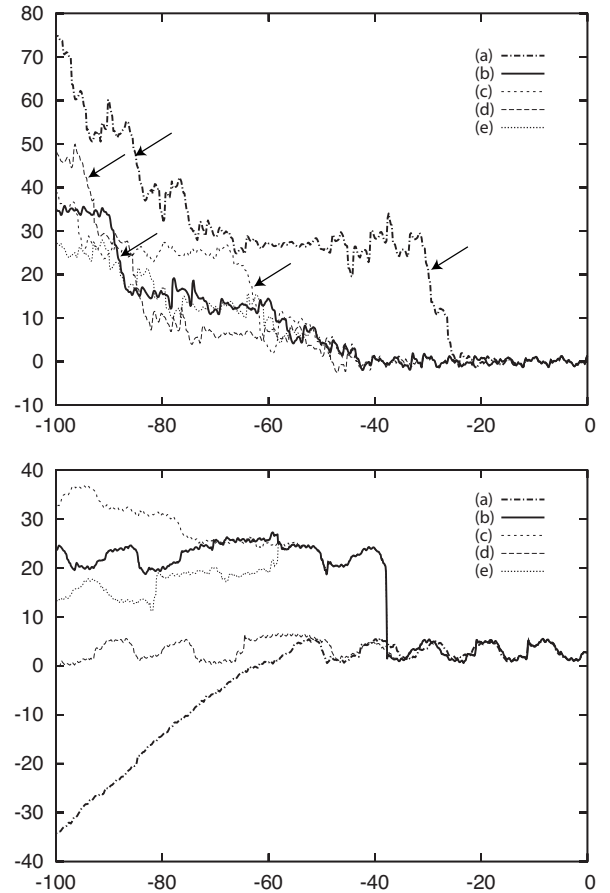


**Fig. 23.** Resonant arguments (in radians versus time in Myr)  $\theta = (s_4 - s_3) - 2(g_4 - g_3)$  (top) and  $\sigma = (g_1 - g_5) - (s_1 - s_2)$  (bottom) for different solutions: **a)** is the secular solution La93 (Laskar 1990; Laskar et al. 1993) while **b)** is the present nominal solution La2004. The characteristics of the other variants La2004<sub>1.5</sub> **c)**, La2004<sub>0</sub> **d)**, La2004\*\* **e)** are listed in Table 9. The arrows indicate the portions of the solutions when the argument  $(s_4 - s_3) - (g_4 - g_3)$  is in libration.

(Laskar 1990, 1992). In Fig. 23 (top), the portions of the solutions where the argument of  $(s_4 - s_3) - (g_4 - g_3)$  is in libration are pointed by arrows. It should be noted that at least over 250 Myr, the diffusion seems to remain confined between the resonances  $(s_4 - s_3) - 2(g_4 - g_3)$  and  $(s_4 - s_3) - (g_4 - g_3)$ . The other important resonant argument  $((g_1 - g_5) - (s_1 - s_2))$  that was identified by Laskar (1990, 1992) as the origin of the chaotic behavior of the inner planets presents in all the variations of the numerical solutions La2004, La2004\*\*, La2004<sub>0</sub>, La2004<sub>1.5</sub> a similar behavior as for the secular solution La93 (Fig. 23 (bottom)).

## 10.2. Geological evidence of chaos

The date of the first transition from libration to circulation of the resonant argument related to  $\theta = (s_4 - s_3) - 2(g_4 - g_3)$  is a macroscopic feature displaying the chaotic diffusion of the planetary orbits. It is thus very tempting to search whether this feature could be observed in the geological data that extend now in continuous records beyond 30 Myr.

The direct observation of the individual arguments related to  $g_3, g_4, s_3, s_4$  is certainly out of reach. But it may be possible to follow the evolution in time of the differences  $g_3 - g_4$  and  $s_3 - s_4$ . Indeed,  $s_3 - s_4$  appears as a beat of about 1.2 million of years in the solution of obliquity, as the result of the beat between the  $p + s_3$  and  $p + s_4$  components of the obliquity, where  $p$  is the precession frequency of the axis (see Laskar 2004, Fig. 7). In a similar way,  $g_3 - g_4$  appears as a beat with period of about 2.4 Myr in the climatic precession. One understands that because of the occurrence of these beats, the detection of the resonant state in the geological data can be possible, as one has to search now for phenomena of large amplitude in the geological signal. Indeed, in the newly collected data from Ocean Drilling Program Site 926, the modulation of 1.2 Myr of the obliquity appears clearly in the spectral analysis of the paleoclimate record (Zachos et al. 2001). Moreover, using the ODP legs 154 and 199, Pälike et al. (2004) could find some evidence that the critical argument of  $\theta$  did not show a transition to circulation at 25 Myr, as in La93, but remained in libration over 40 Myr, as in the present new solution La2004. This result is very impressive, although the search for the determination of these resonant angles in the geological data is just starting. We may expect that a careful analysis, and new data spanning the most recent 60 to 100 Myr, will allow to determine the possible succession of resonant states in the past, allowing, for example, to discriminate between the solutions displayed in Fig. 23. Of particular importance would be the detection of the first transition from libration to circulation of the resonant argument  $(s_4 - s_3) - 2(g_4 - g_3)$ . This program, if completed, will provide some extreme constraint for the gravitational model of the Solar System. Indeed, the observation of a characteristic feature of the solution at 40 to 100 Myr in the past, because of the exponential divergence of the solutions, will provide a constraint of  $10^{-4}$  to  $10^{-10}$  on the dynamical model of the Solar System.

## 11. Mesozoic timescale

An astronomically calibrated time scale for geological data has been achieved successfully over the Neogene period (0–23.03 Myr) (Lourens et al. 2004), and the next challenge will be to improve the astronomical precision of the solution, in order to extend this over the Paleogene (23 to 65 Myr). Beyond this time length, it is hopeless to expect to obtain a precise solution for the orbital elements of the Earth. On the other hand, some features of the solution have a longer time of stability, if they are related to the outer planets secular frequencies (Laskar 1990).

A very important period present in geological records is the 405 kyr period related to the  $g_2 - g_5$  argument, that is the leading term in the solution of eccentricity (Table 6). In Fig. 24, we have tested the stability of this argument over the full period of our integrations, that is over 250 Myr, that extends over the Mesozoic geological era (about 65 to 250 Myr). First, we have compared the argument related to  $g_5$  over 3 variants (La2004\*, La2004<sub>0</sub>, La2004<sub>1.5</sub>) of La2004, that reflect both the numerical errors and the errors of the model. This argument, related to Jupiter and Saturn is extremely stable, and does not show

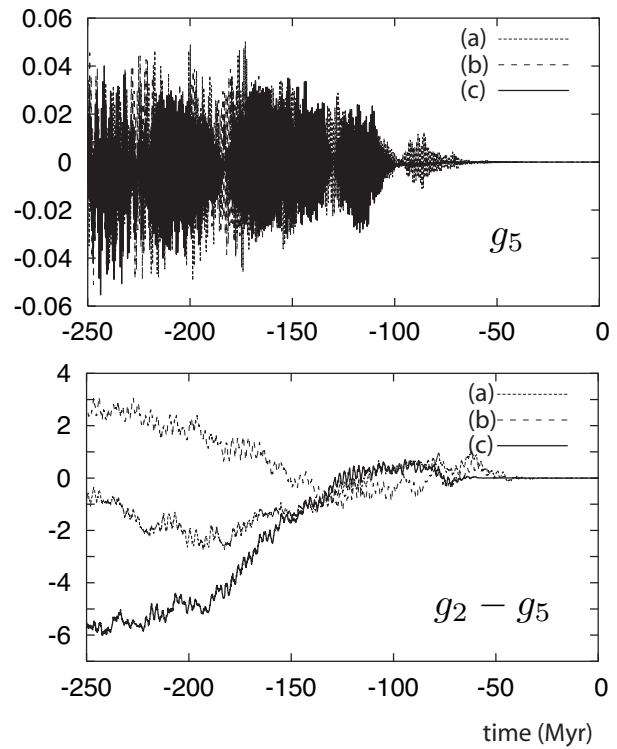


**Fig. 24.** Stability of the  $g_5$  (top) and  $g_2 - g_5$  (bottom) arguments. The difference (in radians) of the angles related to  $g_5$  and  $g_2 - g_5$  from the nominal solution La2004 and an alternate solution La2004<sub>1.5</sub> **a**), La2004<sub>0</sub> **b**), and La2004\* **c**) (Table 9).

variations of more than 0.05 radians over the full 250 Myr period (Fig. 24 (top)). In Fig. 24 (bottom), we have plotted the same quantities for  $g_2 - g_5$ . The dispersions over 50, 100, and 250 Myr are about 0.3, 1.0, 6.2 radians, that correspond to absolute error in time respectively of about 20, 70, and 400 kyr over the same periods.

It is thus possible to use this argument, that is visible in many sedimentary records of the Early Mesozoic (Olsen & Kent 1999, and references therein) as an absolute geological time scale over the whole Mesozoic period. In order to facilitate the establishment of this timescale, we have searched for a best fit or the period of this argument over all the solutions of Table 9. Within the uncertainty of this procedure, the best value for the frequency  $g_2 - g_5$  is

$$\nu_{405} = 3.200''/\text{yr} \quad (45)$$

which corresponds exactly to a period

$$P_{405} = 405\,000\text{ yr.} \quad (46)$$

This value differs by less than  $0.001''/\text{yr}$  from the same quantity from Table 6, where the direct output of the frequency analysis is given. We propose here that in the establishment of geological timescales, the value  $3.200''/\text{yr}$  should be used. The maximum error over 50, 100, 200, and 250 Myr should then be less than respectively 30, 150, 350, and 500 kyr. The 405 kyr term is the largest term of the eccentricity solution. In Fig. 26, the eccentricity of the Earth from La2004, filtered in the



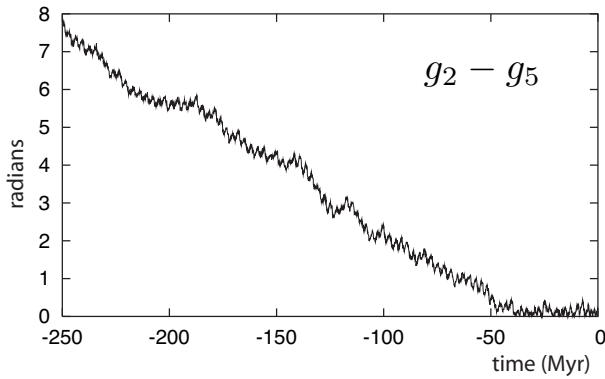


**Fig. 25.** 405 kyr term in eccentricity. Maximum difference (in radians) of the argument  $\theta_{g_2-g_5}$  of  $g_2 - g_5$  in all 6 solutions of Table 9 (La2004, La2004\*, La2004\*\*, La2004<sub>0</sub>, La2004<sub>1.0</sub>, La2004<sub>1.5</sub>) with respect to the linear approximation  $\theta_{g_2-g_5} = 2434'' + 3.200'' t$  where  $t$  is in yr.

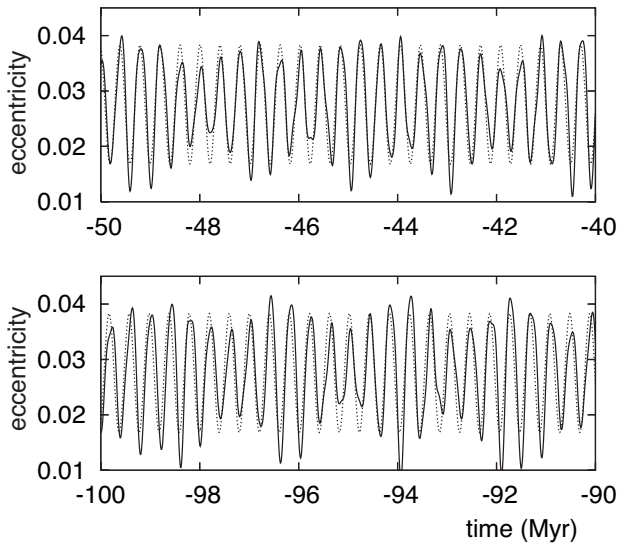


**Fig. 26.** Eccentricity of the Earth. Nominal solution La2004 filtered in the interval  $[2.2''/\text{yr}, 8''/\text{yr}]$  (solid line), and approximation with a single periodic term (47) (dotted line).

interval  $[2.2''/\text{yr}, 8''/\text{yr}]$ , is plotted, as well as a solution for the eccentricity, limited to the single 405 Kyr term

$$e_{405} = 0.027558 - 0.010739 \cos(2434'' + 3.200'' t) \quad (47)$$

where  $t$  is in yr. As it is apparent in the figure, the agreement between the two solutions is extremely good over 100 Myr. Beyond that time, the various possible solutions will become out of phase, within the uncertainty of Fig. 25. One should note that the initial phase at the origin (2434 arcsec) corresponds to an offset of only 760 yr, so in most cases it can be neglected.

## 12. Discussion and future work

### 12.1. Discussion

The new orbital solution of the Earth that is presented here can be used for paleoclimate computations over 40 to 50 Myr. Beyond that time interval, the precision

of the solution cannot be guaranteed but we nevertheless provide the solution over 100 Myr on our Web site [www.imcce.fr/Equipes/ASD/insola/earth/earth.html](http://www.imcce.fr/Equipes/ASD/insola/earth/earth.html) as reference, and for a possible use, with caution, over the full Paleogene period (up to 65 Myr). As in Laskar et al. (1993), the solution for precession and obliquity is not as accurate as the orbital solution. This is mainly due to the uncertainty that remains in the tidal dissipation in the Earth–Moon system. We expect the present solution to be precise over about 20 Myr (see Sect. 9.2), but additional work is certainly needed here.

When taking into account the dissipation in the Earth–Moon system, it is remarkable that in the time interval  $[-250 \text{ Myr}, +250 \text{ Myr}]$ , the only major event in the obliquity of the Earth occurs in the vicinity of the present time (Fig. 14). We have discarded the possibility of some numerical artefact by integrating different models. In particular, we find the same slow decrease of about 0.38 degrees in the obliquity over about 20 Myr either when we integrate the obliquity and precession equations of Sect. 4 at the same time as the orbital equations, or when the precession and obliquity are computed afterwards, with a forced orbital motion. Moreover, the behavior of the solution is perfectly explained by the crossing of the  $s_6 + g_5 - g_6$  resonance, as it is explicated in full details in the appendix.

The crossing of this resonance will occur in the next 20 Myr, but one could wonder whether this crossing could have also occurred in the recent past and thus had a possible impact on the past Earth climate.

In (Laskar et al. 1993), we searched for the possibility to encounter this resonance in the past by changing the momentum of inertia of the Earth as a result of the ice load changes occurring during an ice age, but it seems that our values for the change of momentum of inertia during an ice age was overestimated (Mitrovia & Forte 1995; Levrard & Laskar 2003). In a similar way, Forte & Mitrovia (1997) have advocated the mantle convection as a mean to change the values of the momentum of inertia of the Earth in the past, and thus to eventually cross the  $s_6 + g_5 - g_6$  resonance in the past. Their results are very sensitive to their models, and it is not clear that the induce change of momentum of inertia will be able to counteract the effect of tidal dissipation that drives the obliquity away from the resonance in the past. Moreover, the analysis of geological data in the past few Myr (Lourens et al. 2001; Pälike & Shackleton 2001) tends to show that the precession frequency has actually increased in the past and thus, that the system was driven away from the resonance. Additional studies on this topic are certainly welcome, and we should still search for the possibility of a crossing of the  $s_6 + g_5 - g_6$  resonance in the past, as it may have impacted the climatic history of the Earth, but in absence of new evidence, we should consider that the proximity of this resonance is pure coincidence.

### 12.2. Future work

The next step for the improvement of the solutions will be to obtain an accurate orbital solution over the full Paleogene period (65 Myr). The numerical accuracy of our integrator

already fulfills this requirement (Fig. 23), although we expect to slightly improve it by switching to extended computer precision.

The improvement of the model and parameters is much more difficult, and will require additional work. First, we will have to include in our model supplementary contributions in order to compare much more closely to DE406. In particular, in the present work, to save computer time, we had to simplify the interactions in the Earth–Moon system. In the next integration, we will take into account additional contributions in the body body interactions of the Earth–Moon system, and also the libration of the Moon. We will also have to adapt the tidal model in the Earth–Moon system. We will need to take into account the effect of the 5 main asteroids that are present in DE406, and probably derive a small model for the contribution of the 295 additional asteroids that are considered in DE406. Indeed, the consideration of the main asteroids appears as the next most important source of uncertainty for the long term solution (Table 8). Some of the other factors listed in Table 8 can easily be taken into account, as the consideration of the main Galilean satellites, or the mass loss of the Sun.

Finally, it will also be important to reestablish the precision of the parameter of the model by a direct comparison to the observations. For this part, we expect to benefit from the effort that is developed at present in our laboratory for the improvement of short time ephemeris devoted to the reduction of Earth based and space missions observations (Fienga & Simon 2004).

The fulfilment of this program will allow to improve on the main limiting factors listed in Table 8. It should be stressed again here that the limiting times listed in Table 8 are somewhat pessimistic. We can thus hope that after completing this effort, the orbital solution may be valid over 50 to 65 Myr.

Nevertheless, although this program may lead to a solution valid over about 60 Myr, obtaining a precise solution for the precession and obliquity of the Earth's axis over 65 Myr is much more difficult, as it will require a modelization of the evolution of the various dissipative contributions (see Sect. 4.1) over this period. An alternate way will be to fit the evolution of the main precession frequency to the geological data over the Paleogene period. Although some results have been already obtained in this direction over some shorter time span (Lourens et al. 2001; Pälike & Shackleton 2001), to extract the variation of the precession frequency from paleoclimate stratigraphic data is still a challenge, but we hope that the present paper will provide a good basis for this future work.

## Appendix A: Fresnel integrals and resonances

In this section, we show that Fresnel integrals are very good approximations for the crossing of the resonance. Let us define the Fresnel integrals (we have dropped here the usual  $\pi/2$  factor) as

$$C(x) = \int_0^x \cos(t^2) dt; \quad S(x) = \int_0^x \sin(t^2) dt. \quad (\text{A.1})$$

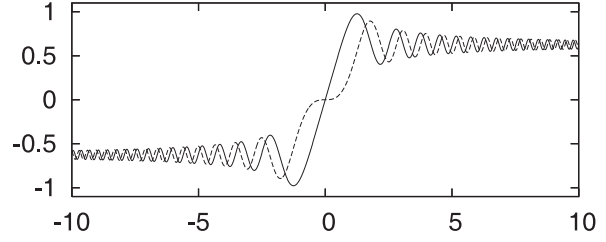


Fig. A.1. Fresnel functions  $C(x)$  (solid line) and  $S(x)$  (dotted line).

We have the expansions, for  $x \geq 0$  (Abramowitz & Stegun 1965)

$$\begin{aligned} C(x) &= \frac{1}{2} \sqrt{\frac{\pi}{2}} - P(x) \cos x^2 + Q(x) \sin x^2 \\ S(x) &= \frac{1}{2} \sqrt{\frac{\pi}{2}} - P(x) \cos x^2 - Q(x) \sin x^2 \end{aligned} \quad (\text{A.2})$$

with the asymptotic expansions

$$\begin{aligned} P(x) &\approx \frac{1}{2} \left( \frac{1}{2x^3} - \frac{1.3.5}{2^3 x^7} + \dots \right) \\ Q(x) &\approx \frac{1}{2} \left( \frac{1}{x} - \frac{1}{2^2 x^5} + \frac{1.3.5.7}{2^4 x^9} + \dots \right). \end{aligned} \quad (\text{A.3})$$

We thus have a jump from the asymptotic value at  $-\infty$  to the value at  $+\infty$  of  $\sqrt{\pi/2} \approx 1.253$  (Fig. A.1). Due to tidal dissipation, the precession angle evolves in first approximation as Eq. (34)

$$\psi = \psi_0 + p_0 T + p_1 T^2 \quad (\text{A.4})$$

with this evolution, a term of frequency  $\nu_k + p$  in Eq. (30) may cross the resonance. In particular, we can compute the contribution of the term  $\nu_{23}$  in the quasiperiodic decomposition of  $\zeta$  (Table 5). We will have from Eq. (28),

$$\left. \frac{d\epsilon}{dt} \right|_{23} = -2a_{23}\nu_{23} \sin((\nu_{23} + p_0)t + p_1 t^2 + \phi_{23} + \psi_0). \quad (\text{A.5})$$

More generally, for  $a > 0$ , the integral of

$$\sin(at^2 + bt + c) \quad (\text{A.6})$$

is

$$\frac{1}{\sqrt{a}} \left( \cos(\delta) S \left( \left( x + \frac{b}{2a} \right) \sqrt{a} \right) + \sin(\delta) C \left( \left( x + \frac{b}{2a} \right) \sqrt{a} \right) \right), \quad (\text{A.7})$$

where  $\delta = c - b^2/4a$ , and the asymptotic offset  $\Delta^{(\epsilon)}$  due to the crossing of the resonance of the term (A.6) is easily obtained as

$$\Delta^{(\epsilon)} = \sqrt{\frac{\pi}{a}} \cos \left( \delta - \frac{\pi}{4} \right). \quad (\text{A.8})$$

With the data for the resonant term  $\nu_{23}$ , we have

$$a = p_1; \quad b = \nu_{23} + p_0; \quad c = \phi_{23} + \psi_0, \quad (\text{A.9})$$

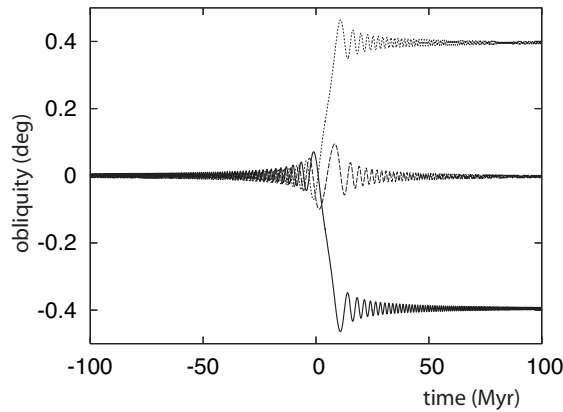


**Fig. A.2.** Obliquity variation (in degree) versus time resulting from the crossing of the resonance in the  $\nu_{23}$  term (solid line). In the same plot, the dependence of the precession phase is illustrated: for  $\delta = -\pi/4$  the obliquity offset is null (dashed line) while it is maximal for  $\delta = +\pi/4$ . The nominal solution (solid line) corresponds nearly to a maximal decrease of the obliquity.

and as the term is of amplitude  $-2a_{23}\nu_{23}$ , we obtain (Fig. A.2) an offset of amplitude

$$\Delta_{23}^{(\varepsilon)} \approx -0.398046 \text{ deg} \quad (\text{A.10})$$

that is very close to the value 0.377602 deg obtained in Sect. 8.3 for the complete integration. It should be noted that the amplitude of the offset depends critically of the phase  $c = \phi_{23} + \psi_0$ . Indeed, a maximum amplitude for the offset will be obtained when  $\delta = \pi/4 \text{ mod}(\pi)$ , which leads to

$$|\Delta_{23}^{(\varepsilon)}|_{\text{max}} = 2a_{23}\nu_{23} \sqrt{\pi/p_1} \approx 0.398721 \text{ deg.} \quad (\text{A.11})$$

while no offset will occur when  $\delta = -\pi/4 \text{ mod}(\pi)$ . In the present case, the actual value of the offset is thus close to its maximum possible value. One should also note that apart from the drift that occurs at the resonance, which ranges from about  $-0.4$  to  $+0.4$  degree, the maximum oscillation of the obliquity is of about 0.1 degree (Fig. A.2).

**Acknowledgements.** J.L. thanks J. Landwehr for providing a copy of Pilgrim's work, A. Vernekar for a copy of his monograph, and H. Pälke for his comments. This work benefited from support from INSU-CNRS, PNP-CNRS, and CS, Paris Observatory.

## References

- Adhémar, J. 1842, *Révolutions de la mer*, (Paris: Bachelier)
- Agassiz, L. 1840, *Études sur les glaciers* (Paris)
- Arnold, V. I., Kozlov, V. V., & Neishtadt, A. I. 1988, *Mathematical aspects of classical and celestial mechanics*, Dyn. Systems III, ed. V. I. Arnold (New York: Springer)
- Berger, A. L. 1978, *J. Atmos. Sci.*, 35, 2362
- Bills, B. G. 1994, *Geophys. Res. Lett.*, 21(3), 177
- Bretagnon, P. 1974, *A&A*, 30, 141
- Bretagnon, P. 1984, *Celest. Mech.*, 34, 193
- Bretagnon, P., & Simon, J.-L. 1990, *A&A*, 239, 387
- Brouwer, D., & Van Woerkom, A. J. J. 1950, *Astron. Papers Am. Ephem.*, XIII, Part II, 81
- Chapman, S., & Lindzen, R. S. 1970, *Atmospheric tides* (Dordrecht: D. Reidel)
- Chirikov, B. 1979, *Phys. Rep.*, 52, 263
- Correia, A., & Laskar, J. 2003, *J. Geophys. Res.*, 108(E11), 5123
- Correia, A., Laskar, J., & Néron de Surgy, O. 2003, *Icarus*, 163, 1
- Croll, J. 1890, *Climate and Time* (London)
- Darwin, G. H. 1880, *Philos. Trans. R. Soc. London*, 171, 713
- Dickey, J. O., Bender, P. L., Faller, et al. 1994, *Science*, 265, 182
- Duriez, L. 1977, *A&A*, 54, 93
- Egbert, G. D., & Ray, R. D. 2000, *Nature*, 405, 775
- Fienga, A., & Simon, J.-L. 2004, submitted
- Forte, A., & Mitrovica, J. X. 1997, *Nature*, 390, 676
- Gradstein, F., Ogg, J., & Smith, A. 2004, *A Geologic Time Scale 2004* (UK: Cambridge University Press), in press
- Haretu, S. C. 1885, *Annales de l'Observatoire de Paris*, 18, II
- Harzer, P. 1895, *Die Säcularen veränderungen der bahnen der grossen planeten*, Fürstlich Jablonowski'schen Gesellschaft, Leipzig
- Hays, J. D., Imbrie, J., & Shackleton, N. J. 1976, *Science*, 194, 1121
- Hill, G. 1897, *AJ*, 17(11), 81
- Imbrie, J. 1982, *Icarus*, 50, 408
- Imbrie, J., & Imbrie, K. P. 1979, *Ice Ages: Solving the Mystery* (MA: Harvard University Press)
- Ito, T., & Tanikawa, K. 2002, *MNRAS*, 336, 483
- Ito, T., Masuda, K., Hamano, Y., & Matsui, T. 1995, *J. Geophys. Res.*, 100, 15147
- Jeffreys, H. 1920, *Phil. Trans. R. Soc. London, Ser. A*, 221, 239
- Jeffreys, H. 1976, *The Earth, Its Origin, History, and Physical Constitution*, 6th ed. (Cambridge, UK: Cambridge University Press)
- Kinoshita, H. 1977, *Cel. Mech.*, 15, 277
- Lagrange, J. L. 1774, *Oeuvres complètes*, t. IV, Gauthier-Villars, Paris, 1869, 111
- Lagrange, J. L. 1776, *Oeuvres complètes*, t. IV, Gauthier-Villars, Paris, 1869, 255
- Lagrange, J. L. 1777, *Oeuvres complètes*, t. VI, Gauthier-Villars, Paris, 1873, 633
- Lagrange, J. L. 1781, *Oeuvres complètes*, t. V, Gauthier-Villars, Paris, 1870, 125
- Lagrange, J. L. 1782, *Oeuvres complètes*, t. V, Gauthier-Villars, Paris, 1870, 211
- Lambeck, K. 1980, *The Earth's variable rotation* (UK: Cambridge University Press)
- Lambeck, K. 1980, *Geophysical Geodesy* (UK: Oxford University Press)
- Laplace, P. S. 1773–1776, *Oeuvres complètes*, t. VIII, Gauthier-Villars, Paris, 1891, 199
- Laplace, P. S. 1776, *Oeuvres complètes*, t. VIII, Gauthier-Villars, Paris, 1891, 369
- Laskar, J. 1984, *Théorie générale planétaire: Eléments orbitaux des planètes sur 1 million d'années*, Thèse, Observatoire de Paris
- Laskar, J. 1985, *A&A*, 144, 133
- Laskar, J. 1986, *A&A*, 157, 59
- Laskar, J. 1988, *A&A*, 198, 341
- Laskar, J. 1989, *Nature*, 338, 237
- Laskar, J. 1990, *Icarus*, 88, 266
- Laskar, J. 1992, in *Chaos, resonance and collective dynamical phenomena in the solar system*, Ferraz-Mello, S. (1) (Kluwer Acad. Publ.), IAU Symp., 152
- Laskar, J. 1999, *Phil. Trans. R. Soc. Lond. A.*, 357, 1735
- Laskar, J. 1999, *Introduction to frequency map analysis*, in NATO ASI 533 3DHAM95, S'Agaró, Spain, C. Simò (Kluwer), 134
- Laskar, J. : 2001, *Astronomical Solutions for Paleoclimate Studies*, AGU Fall Meeting 2001 Abstracts U11A-01
- Laskar, J. 2003, *Ann. Henri Poincaré*, 4, Suppl. 2, S693
- Laskar, J. 2003, in *Hamiltonian systems and Fourier analysis*, ed. Benest et al. (Taylor, Francis), in press

- Laskar, J., Joutel, F., & Boudin, F. 1993, *A&A*, 270, 522
- Laskar, J., & Robutel, P. 2001, *Celest. Mech.*, 80, 39
- Laskar, J., Correia, A. C. M., Gastineau, M., et al. 2004, *Icarus*, 170, 343
- Le Verrier, U. 1856, *Ann. Obs. Paris*, II, Mallet-Bachelet, Paris
- Levrard, B., & Laskar, J. 2003, *Journal Geophys. Int.*, 154, 970
- Lourens, L. J., Wehausen, R., & Brumsack, H. J. 2001, *Nature*, 409, 1029
- Lourens, L. J., Hilgen, F. J., Shackleton, N. J., Laskar, J., & Wilson, D. 2004, in *The Neogene Period*, ed. F. Gradstein, J. Ogg, & A. Smith, *A Geologic Time Scale 2004* (UK: Cambridge University Press), in press
- Lumb, L. I., & Aldridge, K. D. 1991, *J. Geomagn. Geoelectr.*, 43, 93
- MacCarthy, D. D. 1992, *IERS Standards*, IERS Technical note 13, Observatoire de Paris
- MacCarthy, D. D., & Petit, G. 2004, *IERS Standards*, IERS Technical note 13, Observatoire de Paris
- Mignard, F. 1979, *The Moon and the Planets*, 20, 301
- Mignard, F. 1980, *The Moon and the Planets*, 23, 185
- Mignard, F. 1981, *The Moon and the Planets*, 24, 189
- Milani, A., Nobili, A. N., & Carpino, M. 1987, *A&A*, 172, 265
- Milankovitch, M. 1941, *Kanon der Erdbestrahlung und seine Anwendung auf das Eiszeitenproblem*, Royal Serbian Academy
- Mitrovica, J. X., & Forte, A. 1995, *Geophys. J. Int.*, 121, 21
- Néron de Surgy, O., & Laskar, J. 1997, *A&A*, 318, 975
- Newhall, X. X., Standish, E. M., & Williams, J. G. 1983, *A&A*, 125, 150
- Olsen, P., & Kent, D. 1999, *Phil. Trans. R. Soc. London, Ser. A.*, 357, 1761
- Pälike, H. 2002, Thesis, University of Cambridge
- Pälike, H., & Shackleton, N. J. 2001, *EPSL*, 400, 1029
- Pälike, H., Laskar, J., & Shackleton, N. J. 2004, *Geological constraints on the chaotic diffusion of the Solar System*, *Geology*, in press
- Pijpers, F. P. 1998, *MNRAS*, 297, L76
- Pilgrim, L. 1904, *Versuch einer rechnerischen behandlung des eiszeitenproblems. Jahreshefte für vaterlandische Naturkunde in Württemberg*, 60
- Poincaré, H. 1893, *Méthodes nouvelles de la mécanique céleste*, (Paris: Gauthier-Villars), Vol. II
- Poincaré, H. 1910, *Bull. Astron.*, 27, 321
- Pontécoulant, G. de 1834, *Théorie Analytique du Système du Monde*, t. III, Bachelier, Paris
- Quinn, T. R., Tremaine, S., & Duncan, M. 1991, *AJ*, 101, 2287
- Rochester, M. G. 1976, *Geophys. J. R. A. S.*, 46, 109
- Rubincam, D. P. 1990, *Science*, 248, 720
- Rubincam, D. P. 1995, *Paleoceanography*, 10, 365
- Saha, P., & Tremaine, S. 1994, *AJ*, 108 (5), 1962
- Sharav, S. G., & Boudnikova, N. A. 1967a, *Bull. I.T.A*, XI-4(127), 231
- Sharav, S. G., & Boudnikova, N. A. 1967b, *Trud. I.T.A*, XIV, 48
- Standish, E. M. 1998, *JPL planetary and Lunar ephemerides*, DE405/LE405. JPL IOM 312.F-98-048, Pasadena
- Stockwell, J. N. 1873, *Memoir on the secular variations of the elements of the eight principal planets*. Smith. Contr. Knowledge, Washington, 18
- Sussman, G. J., & Wisdom, J. 1992, *Science*, 257, 56
- Touma, J., & Wisdom, J. 1994, *AJ*, 108, 1943
- Varadi, F., Bunnegar, B., & Ghil, M. 2003, *ApJ*, 592, 620
- Vernekar 1972, *Long-period global variations of incoming solar radiation*, *Meteorol. Monogr.*, 12
- Volland, H. 1978, *Earth's rotation from eons to days*, ed. Brosche and Sündermann (Springer), 62
- Williams, D. M., Kasting, J. F., & Frakes, L. A. 1998, *Nature*, 396, 453
- Williams, J. G., Boggs, D. H., Yoder, C. F., Ratcliff, J. T., & Dickey, J. O. 2001, *J. Geophys. Res.*, 106, 27933
- Wisdom, J., & Holman, M. 1991, *AJ*, 102(4), 128
- Yoder, C. F. 1995, *Astrometric and geodetic properties of Earth and the Solar System*, in ed. T. J. Ahrens, *Global Earth Physics: A Handbook of Physical Constants*, American Geophysical Union, Washington DC, 1
- Zachos, J. C., Shackleton, N. J., Revenaugh, J. S., Pälike, H., & Flower, B. P. 2001, *Science*, 292, 274
- Zachos, J. C., Pagani, M., Sloan, L., Thomas, E., & Billups, K. 2001, *Science*, 292, 686